



**HAL**  
open science

## Clinically approved IVIg delivered to the hippocampus with focused ultrasound promotes neurogenesis in a model of Alzheimer's disease

Sonam Dubey, Stefan Heinen, Slavica Krantic, Joanne Mclaurin, Donald Branch, Kullervo Hynnen, Isabelle Aubert

### ► To cite this version:

Sonam Dubey, Stefan Heinen, Slavica Krantic, Joanne Mclaurin, Donald Branch, et al.. Clinically approved IVIg delivered to the hippocampus with focused ultrasound promotes neurogenesis in a model of Alzheimer's disease. *Proceedings of the National Academy of Sciences of the United States of America*, 2020, 117 (51), pp.32691-32700. 10.1073/pnas.1908658117 . hal-03091324

**HAL Id: hal-03091324**

**<https://hal.science/hal-03091324>**

Submitted on 4 Jan 2021

**HAL** is a multi-disciplinary open access archive for the deposit and dissemination of scientific research documents, whether they are published or not. The documents may come from teaching and research institutions in France or abroad, or from public or private research centers.

L'archive ouverte pluridisciplinaire **HAL**, est destinée au dépôt et à la diffusion de documents scientifiques de niveau recherche, publiés ou non, émanant des établissements d'enseignement et de recherche français ou étrangers, des laboratoires publics ou privés.

1 **TITLE**

2 Clinically approved IVIg delivered to the hippocampus with focused ultrasound promotes  
3 neurogenesis in a model of Alzheimer's disease

4

5 **Authors**

6 Sonam Dubey<sup>1,2</sup>, Stefan Heinen<sup>1</sup>, Slavica Krantic<sup>3</sup>, JoAnne McLaurin<sup>1,2</sup>, Donald Branch<sup>2</sup>,  
7 Kullervo Hynynen<sup>4,5</sup>, \*Isabelle Aubert<sup>1,2</sup>

8

9 **Affiliations**

- 10 1. Biological Sciences, Hurvitz Brain Sciences Research Program, Sunnybrook Research  
11 Institute, Toronto, ON, Canada
- 12 2. Laboratory Medicine and Pathobiology, University of Toronto, ON, Canada
- 13 3. INSERM UMRS 938, Saint Antoine Research Center, Paris, France
- 14 4. Physical Sciences, Sunnybrook Research Institute, Toronto, ON, Canada
- 15 5. Medical Biophysics, University of Toronto, Toronto, ON, Canada

16

17 **\*Corresponding Author**

18 Dr. Isabelle Aubert

19 Email: [isabelle.aubert@utoronto.ca](mailto:isabelle.aubert@utoronto.ca)

20 Phone: 416-480-6100 x 5831

21 Fax: 416-480-573

**22 Abstract (250 words max)**

23 Preclinical and clinical data support the use of focused ultrasound (FUS), in presence of  
24 intravenously injected microbubbles, to safely and transiently increase the permeability of the  
25 blood-brain barrier (BBB). FUS-induced BBB permeability can enhance the bioavailability of  
26 therapeutics the brain. FUS-mediated delivery requires the intravenous administration of  
27 therapeutics. Therefore, therapeutics capable of inducing benefits peripherally and at FUS-targeted  
28 brain areas are ideal candidates. In Alzheimer's disease, intravenous immunoglobulin (IVIg), a  
29 fractionated human blood product containing polyclonal antibodies, act as immunomodulator  
30 peripherally and centrally, and it can reduce amyloid pathology in the brain. Using the TgCRND8  
31 mouse model of amyloidosis, we tested whether FUS can improve the delivery of IVIg,  
32 administered intravenously (0.4 g/kg), to the hippocampus and reach an effective dose to reduce  
33 amyloid plaque pathology and promote neurogenesis. Our results show that FUS-induced BBB  
34 permeability is required to deliver a significant amount of IVIg (489 ng/mg) to the targeted  
35 hippocampus of TgCRN8 mice. Two IVIg-FUS treatments, administered at day 1 and 8,  
36 significantly increased hippocampal neurogenesis by 4-, 3- and 1.5-fold in comparison to saline,  
37 IVIg alone, and FUS alone, respectively. Amyloid plaque pathology was significantly reduced in  
38 all treatment groups; IVIg alone, FUS alone, and IVIg-FUS. Putative factors promoting  
39 neurogenesis in response to IVIg-FUS include the downregulation of the pro-inflammatory  
40 cytokine tumor necrosis factor alpha in the hippocampus. In summary, FUS was required to deliver  
41 an effective dose of IVIg to the targeted hippocampus, where IVIg could then promote  
42 neurogenesis and modulate the inflammatory milieu.

**43 Keywords**

44 Alzheimer's disease, immunotherapy, MRI-guided focused ultrasound, blood-brain barrier,  
45 intravenous immunoglobulin, mouse model of amyloidosis, neurogenesis.

46 **Significance Statement (120 words max)**

47       The efficacy of immunotherapy in Alzheimer's disease is limited; partly because antibodies,  
48 administered peripherally, have poor access to the brain. Focused ultrasound with microbubbles  
49 allows the passage of antibodies from the blood to the brain. In a mouse model of Alzheimer's  
50 disease, antibodies administered in the blood, with and without focused ultrasound, reduced  
51 amyloid pathology in the hippocampus. In contrast, focused ultrasound was required to deliver  
52 sufficient antibodies to effectively promote hippocampal neurogenesis. Neurogenesis, a  
53 regenerative process involved in memory functions, is impaired in Alzheimer's disease. Putative  
54 contributors to the stimulation of neurogenesis include a decrease in the proinflammatory cytokine  
55 tumor necrosis factor alpha. Focused ultrasound holds potential to increase the efficacy of  
56 immunotherapy for Alzheimer's disease.

57

## 58 **Introduction**

59 Alzheimer's Disease (AD) is a neurodegenerative disease estimated to affect 132 million  
60 individuals worldwide by 2050. The incidence of AD significantly increases with age, with one in  
61 10 people over 65-year-old being affected (1). At present, AD has no cure and the multifaceted  
62 nature of this disorder prompts the development of therapeutics that can both reduce pathologies  
63 and promote the regenerative capacity of the brain (2).

64 One such therapeutic is intravenous immunoglobulin (IVIg). IVIg is composed of pooled  
65 antibodies collected from healthy blood donors that have been shown, in patients with AD and/or  
66 animal models of AD, to decrease amyloid-beta peptides (A $\beta$ ) and tau pathology, dampen  
67 excessive inflammation, and increase neurogenesis (3-11). The excellent safety profile of IVIg  
68 combined with its beneficial effects, in animal models and early clinical AD trials, led to a Phase  
69 III trial in patients with mild to moderate AD (12, 13). The Phase III clinical trial failed to  
70 demonstrate significant cognitive improvement in the overall population treated, although a  
71 subgroup analysis pointed to some benefits in apolipoprotein-E4 carriers and at moderate AD  
72 stages (8, 12-14).

73 The properties of the blood-brain barrier (BBB) restrict the bioavailability of IVIg to the  
74 brain. While technically difficult to evaluate in human, studies in murine models of AD have  
75 shown that less than 0.002% of intravenous IVIg reach the hippocampus (8, 12, 13, 15). Using  
76 higher dosages to increase the amount of IVIg to the brain has limitations, both in terms of safety  
77 and feasibility. Clinically, IVIg is used for several autoimmune and inflammatory conditions, and  
78 its expansion to AD at relatively high dosages could put a serious burden on the provision of IVIg,  
79 a human source biologic (16, 17). As such, strategies are warranted to develop recombinant  
80 alternatives to IVIg (18), reduce the amount of IVIg required intravenously, and combine IVIg  
81 with new therapeutic and delivery approaches to increase efficacy. The present study contributes

82 to efforts in improving treatment efficacy by enhancing the delivery of IVIg to the brain using  
83 focused ultrasound (FUS), keeping a relatively low dose of IVIg administered intravenously, and  
84 potentially benefiting from FUS-induced effects in reducing pathology and increasing  
85 neurogenesis (19) (20-22).

86 Since 2001, MRI-guided FUS, combined with intravenously administered microbubbles, has  
87 been established as a modality to increase the permeability of the BBB (23). The use of well-  
88 defined FUS parameters, microbubbles dosage, an acoustic emissions-based controller, and MRI  
89 guidance provides assurance, in real-time, that FUS-induced BBB permeability is done in a safe,  
90 controlled, and targeted manner (23-29). FUS-mediated drug delivery requires the administration  
91 of therapeutics intravenously to facilitate their passage through the BBB and into the brain at FUS-  
92 targeted regions. Therefore, therapeutics which are beneficial centrally and peripherally, such as  
93 IVIg (8, 17), are ideal candidates to combine with FUS-mediated drug delivery. To date,  
94 molecules, cells and gene vectors have been shown to be effectively delivered using FUS (26). In  
95 animal models of AD, FUS-mediated drug delivery to the brain has been used for  
96 immunotherapy against A $\beta$  and tau pathologies (30-33), and for the delivery of a specific agonist  
97 stimulating TrkA signaling and acetylcholine release (34).

98 We hypothesized that FUS-induced BBB permeability would significantly enhance the  
99 delivery of IVIg from the blood to the hippocampus, a brain region vulnerable in AD (35), and  
100 thereby improve treatment efficacy. To test this hypothesis, we used the transgenic murine model  
101 of amyloidosis, namely TgCRND8, starting at 3 months of age. At this age, TgCRND8 mice  
102 display salient features of AD, such as A $\beta$  plaque burden (36), glial activation (37) associated with  
103 increased tumor necrosis factor alpha (TNFa) (38), impaired hippocampal neurogenesis and  
104 function (39, 40). As such, TgCRND8 mice at 3-months of age model a clinical stage when  
105 patients would be presenting with pathological characteristics of AD, and prior to further neuronal

106 systems degenerating (41, 42). Evidence suggests that treating AD at relatively early stages may  
107 be more efficient than at the later stages, when neurodegeneration reaches irreversible stage (43).

108 In the present study, we first demonstrated the feasibility of IVIg delivery to the  
109 hippocampus using MRI-guided FUS in TgCRND8 mice. We next assessed the timeline of IVIg  
110 clearance from the brain. Finally, therapeutic efficacy of two weekly treatments of IVIg, FUS, and  
111 IVIg-FUS (at day 1 and day 8) was investigated two weeks later, at day 21 on A $\beta$  plaque pathology,  
112 neurogenesis and the inflammatory status centrally, in the hippocampus, and peripherally, in the  
113 serum.

## 114 **Results**

### 115 **Focused ultrasound increases the bioavailability of IVIg to the hippocampus**

116 The bioavailability of IVIg delivered to the hippocampus with FUS was measured at 4 hours,  
117 24 hours, 7 days and 14 days post-treatment (Fig 1A), in TgCRND8 (Tg) and non-transgenic (nTg)  
118 mice. Two FUS spots per region were chosen for targeting the left hippocampus, and as a  
119 supplementary region the frontal cortex (Fig. 1B). Under MRI-guidance, the left hippocampus and  
120 cortex were selected (Fig 1C) and targeted with FUS (Fig 1D). The contralateral right hemisphere  
121 served as non-FUS control side, allowing for paired comparison within animals. Both hippocampi  
122 were exposed to IVIg in the circulation (0.4 kg/kg, *i.v.*) and only the left hippocampus was targeted  
123 with FUS.

124 Immediately following FUS treatment in presence of microbubbles (0.02 ml/kg),  
125 gadolinium-based MRI contrast agent, Gadodiamide (GAD) (0.2 ml/kg) and IVIg (0.4 g/kg) were  
126 injected intravenously. To visualize the permeability of the BBB, post-FUS treatment T1-weighted  
127 (w) images (e.g. Fig 1D) were compared to the pre-FUS T1w images (e.g. Fig 1C). BBB  
128 permeability at the target locations was confirmed by GAD enhancement on T1w images post-  
129 FUS, as noted by the two lighter gray spots in the hippocampus and in the cortex in Fig 1D

130 compared to Fig 1C. The levels of enhancement produced by GAD at FUS sites was not  
131 significantly different between Tg and nTg animals (Fig 1E, n=16, p= 0.21), indicating that the  
132 levels of BBB permeability induced by FUS is comparable in Tg and nTg mice.

133 In Tg mice, IVIg at 0.4 g/kg (12 mg per mouse, *i.v.*) did not bypass the BBB in the absence  
134 of FUS (Fig 1F, 4-hour time-point, n=6, 0 ng/mg). In contrast, in FUS-targeted hippocampi the  
135 levels of IVIg detected 4 hours post-treatment ranged from 67 to 1,013 ng/mg. and on average  
136 (489 ng/mg) significantly higher compared to the untreated side (average 0 ng/mg) (Fig 1F,  
137 p=0.016, n=6). Therefore, our bioavailability data demonstrate that one administration of IVIg-  
138 FUS delivered represent, on average, 0.09% (0.01 to 0.2%) of the injected dose to the targeted  
139 hippocampi. At 24 hours post-FUS, IVIg remaining in the targeted hippocampi averaged 152  
140 ng/mg (Fig 1F, p=0.063 compared to the untreated side, average 0 ng/mg, n=6). By 7 and 14 days  
141 less than 20 ng/mg were detected on the FUS-treated hippocampus of Tg mice (Fig 1F, n=6 per  
142 group).

143 In nTg animals, the levels of IVIg in the FUS treated hippocampi averaged 333 ng/mg,  
144 approximately 0.06% of the injected dose, compared to 76 ng/mg on the contralateral untreated  
145 side (Fig 1G, p=0.016, n=6), and they remained elevated at 24 hours in FUS treated hippocampi  
146 (311 ng/mg) compared to the untreated side (90 ng/mg) (Fig 1G, p=0.016, n=6.). The levels of  
147 IVIg remaining in the hippocampus post-FUS at 7 (62 ng/mg) and 14 (6 ng/mg) days were not  
148 statistically different than those observed on the contralateral side; respectively 24 ng/mg (Fig 1G,  
149 p=0.063, n=6 ) and 2 ng/mg (Fig 1G, p=0.125, n=6). The same trends were observed for the  
150 delivery of IVIg to the FUS-treated cortex of Tg and nTg mice (S1A, B, n=6 per group).

151 We next evaluated the biological effects of IVIg-FUS treatments on A $\beta$  plaque pathology,  
152 neurogenesis and inflammation. Bilateral hippocampal targeting was done for the following  
153 reasons: to cover the entire region for quantification of A $\beta$  plaque pathology, to provide an

154 appropriate sampling area for the estimation of the total number of cells undergoing hippocampal  
155 neurogenesis per animal and to globally treat the hippocampus for potential impact on serum  
156 CCTF levels. Based on the clearance of IVIg at 7 days post-FUS treatment (Fig 1F, G), sex-  
157 balanced and age matched Tg and nTg animals received two weekly treatments (Fig 2A, B), being  
158 allocated to one of four cohort: saline, IVIg, FUS or IVIg-FUS. To confirm that the increased BBB  
159 permeability post-FUS is consistent between Tg and nTg animals, pre-T1w (Fig 2C) and post-T1w  
160 (Fig 2D) images were analyzed. The increase in gadolinium (GAD) extravasation into the  
161 hippocampus, visualized as the hypointense regions in post-T1w images, was not significantly  
162 different between the FUS treated Tg and nTg animals (Fig 2E, n=10, p=0.33). Therefore,  
163 differences in the biological effects observed under these conditions are unlikely to result from  
164 variability in the extent of FUS mediated BBB permeability between Tg and nTg animals. Two  
165 weekly bilateral treatments of IVIg alone and IVIg-FUS resulted in the immunochemical detection  
166 of IVIg in the hippocampus, 14 days following the last treatment (S2A, B). The human-specific  
167 Ig-immunopositivity in FUS-targeted hippocampi (S2A; c, d) was higher compared to animals that  
168 received IVIg alone (*i.v.* without FUS, S2A, b) (S2B; p<0.05) and saline (S2A, a, B; p<0.01). IVIg  
169 alone (*i.v.* without FUS, S2A, b) also led to levels of human Ig-immunopositivity greater than those  
170 measured in the saline group (S2A, a, B; p<0.05). The immunopositive signal of IVIg in the  
171 hippocampus of Tg mice is diffuse (S2A), with visible binding to A $\beta$  plaques (S2A, d, arrows)  
172 reminiscent of observations made by Puli et al. (9) in APP/PS1dE9 mice.

### 173 **A $\beta$ plaque pathology is reduced by all treatments (IVIg, FUS, and IVIg-FUS)**

174 A $\beta$  plaque pathology was quantified in the hippocampus of Tg animals (saline, Fig 2F; IVIg-  
175 FUS, Fig 2G). A significant reduction in the number of hippocampal plaques was found following  
176 treatments with FUS (n=5, p<0.05), IVIg (n=6, p<0.01) and IVIg-FUS (n=5, p<0.01) compared  
177 to animals receiving saline (n=5, Fig 2J). Similarly, the mean surface area, i.e. plaque load, was

178 significantly lowered in FUS ( $p < 0.01$ ), IVIg ( $p < 0.001$ ), and IVIg-FUS ( $p < 0.001$ ) treated animals  
179 compared to the saline group (Fig 2K). A 68% reduction in plaque load was observed following  
180 IVIg-FUS treatment, compared to saline (Fig 2K). Treatments with IVIg alone and FUS alone  
181 reduced plaque load by 57% and 40%, respectively, compared to saline (Fig 2K). No difference  
182 was observed in the mean plaque size (S2C).

183 Both IVIg-alone and FUS-alone have been independently reported to reduce A $\beta$  plaque  
184 pathology and promote neurogenesis (7, 19-21, 35). As such, we next investigated whether an  
185 increase in neurogenesis in Tg animals could occur with FUS, IVIg and IVIg-FUS treatments, in  
186 addition to a reduction in A $\beta$  plaque pathology,

### 187 **FUS is required for IVIg to promote hippocampal neurogenesis**

188 To evaluate the effects on neurogenesis, we quantified cells labeled with markers of  
189 proliferation (bromodeoxyuridine, BrdU) and immature neurons (doublecortin, DCX) in all groups  
190 (Fig 2H, I; *BrdU*, red; DCX, green). In Tg mice, FUS treatment alone increased the number of  
191 BrdU-positive cells compared to saline ( $p < 0.05$ ) and IVIg alone ( $p < 0.05$ ) (Fig 2L,  $n=5$ ). IVIg-FUS  
192 treatments further increased the number of BrdU-positive cells compared to saline ( $p < 0.0001$ ),  
193 IVIg ( $p < 0.001$ ) and FUS alone ( $p < 0.01$ ) (Fig 2L). Notably, a 3-fold increase in proliferating cells  
194 (BrdU-positive) with IVIg-FUS treatments was found compared to IVIg alone ( $p < 0.001$ ) (Fig 2L).  
195 IVIg-FUS also increased the number of post-treatment proliferating cells maturing towards a  
196 neuronal phenotype (BrdU-positive/DCX-positive) when compared to saline ( $p < 0.01$ ), IVIg  
197 ( $p < 0.01$ ) and FUS ( $p < 0.01$ ) in Tg animals (Fig 2M,  $n=5$ ). The average number of BrdU-  
198 positive/DCX-positive cells was 3-times higher in Tg mice treated with IVIg-FUS compared to  
199 IVIg alone ( $p < 0.05$ ) (Fig 2M). At the dosage of IVIg given intravenously, FUS was required for  
200 IVIg to have beneficial effects on hippocampal neurogenesis. These results contrast with the  
201 significantly reduction in A $\beta$  plaque load observed with IVIg alone. Indeed, with regards to

202 hippocampal neurogenesis IVIg alone did not increase cell proliferation (BrdU-positive) nor cell  
203 differentiation (DCX-positive). Further analysis supported the lack of correlation between A $\beta$   
204 plaque load and hippocampal cell proliferation in Tg animals ( $R^2=0.21$ , *S2D*). Therefore, in this  
205 experimental setting, decreasing A $\beta$  load from a peripheral approach, i.e. with intravenous IVIg  
206 administration, is insufficient to promote neurogenesis.

207 We further demonstrated the necessity of FUS for IVIg-induced hippocampal neurogenesis,  
208 and the concept that this effect is independent of A $\beta$  by using nTg mice, where A $\beta$  pathology is  
209 lacking. In the hippocampus of nTg animals, the number of cells proliferating (BrdU-positive) and  
210 differentiating in a neuronal phenotype (DCX-positive) significantly increased only following  
211 IVIg-FUS treatments, compared to saline ( $p<0.01$ ), FUS ( $p<0.05$ ), and IVIg ( $p<0.01$ ) (Fig 2 *N-O*).

212 Aside from the effects of IVIg on A $\beta$ , IVIg has been characterized as an immunomodulatory  
213 agent (17, 44, 45). Because of the potential influence of IVIg on inflammatory cytokines, key  
214 modulators of neurogenesis (46), we next investigated whether treatments with IVIg and FUS  
215 impacted the inflammatory milieu in a different manner than IVIg alone in Tg mice.

### 216 **IVIg-FUS treatments decrease hippocampal TNF $\alpha$**

217 The choice of investigating changes in the hippocampal inflammatory milieu in response to  
218 treatments was motivated by the finding that IVIg-FUS treatments increased neurogenesis by 3-  
219 fold compared to IVIg treatment alone in Tg mice, and despite comparable ability of IVIg alone  
220 and IVIg-FUS to reduce A $\beta$  plaque pathology. Therefore, in an exploratory study design (47), we  
221 assessed the levels of cytokines, chemokines and trophic factors (CCTFs)—which could be  
222 responsible for the increase of hippocampal neurogenesis— in Tg mice treated with IVIg, with and  
223 without FUS.

224 Using multiplex laser bead ELISA assay, of the 36 CCTF studied, 14 had detectable levels  
225 in the hippocampal formation (Fig 3A, B, S3). Among these, only TNF $\alpha$  and CCL5 responded

226 differently to IVIg-FUS compared to IVIg alone treatments in Tg mice (Fig 3A, B). The  
227 hippocampal levels of pro-inflammatory cytokine TNF $\alpha$  were lowered with IVIg-FUS treatment  
228 compared to IVIg (Fig 3A,  $p < 0.05$ ). In contrast, mice treated with IVIg-FUS had elevated levels  
229 of chemokine CCL5 in the hippocampus compared to IVIg alone (Fig 3B,  $p < 0.05$ ).

230 Through the elucidation of CCTFs produced in response to IVIg-FUS and IVIg treatments  
231 in Tg mice, we also uncovered significant changes in CCTFs in our control groups, i.e. in response  
232 to FUS alone, in absence of IVIg (S3). Specifically, FUS treatments induced decreases in IL1 $\alpha$ ,  
233 IL2, TGF $\beta$ 1, TGF $\beta$ 2 in both Tg and non-Tg mice (S3A, B, J, K). As a whole of the panel of CCTFs  
234 studied, changes in CCTFs in responses to all treatments, namely FUS alone, IVIg alone, and IVIg-  
235 FUS were more frequently observed in nTg compared to Tg mice (S3). In summary, IVIg  
236 modulated CCTFs in the hippocampus of Tg mice only when combined with FUS. IVIg-FUS  
237 treatments decreased hippocampal TNF $\alpha$  and increased CCL5 (Fig 3A, B).

238 Because IVIg was administered intravenously and has known peripheral immunomodulatory  
239 effects we also investigated the changes in CCTF levels in the blood. TNF $\alpha$  levels in the serum  
240 were elevated in IVIg-FUS compared to IVIg treated Tg mice (Fig 3C,  $p < 0.05$ ), in contrast with  
241 the results observed in the hippocampus (Fig 3A). CCL5 levels in the serum of Tg animals treated  
242 with IVIg-FUS were significantly higher compared to those treated with IVIg alone (Fig 3D,  
243  $p < 0.05$ ), similarly to the hippocampal response (Fig 3B). Additional differences in CCTFs of IVIg-  
244 FUS treated Tg animals include increased CCL4 (Fig 3E,  $p < 0.05$ ), and decreased CCL7 (Fig 3F,  
245  $p < 0.001$ ), compared to IVIg treatment alone. IL2 and GM-CSF levels between IVIg-FUS and IVIg  
246 treated Tg animals were not statistically different. However, both IVIg-FUS and IVIg treatments  
247 appear to induce CCL4, IL2 and GM-CSF compared to low and undetectable levels in absence of  
248 IVIg (Fig 3E, G, H). In summary, the serum data shows that in Tg mice, FUS treatments combined  
249 with IVIg, administered intravenously, differentially alters the blood levels of the CCTFs TNF $\alpha$ ,

250 CCL4, 5, and 7 compared to IVIg alone (Fig 3C-F). Such differential alteration of blood CCTFs  
251 between IVIg-FUS and IVIg treatments in Tg mice was not observed for IL2 and GM-CSF (Fig  
252 3G, H).

253 Taken together, these results highlight the profile of CCTFs in response to IVIg-FUS  
254 compared to IVIg in Tg mice centrally (FUS-targeted hippocampus, e.g. decrease in TNF $\alpha$ ) and in  
255 the periphery (serum, e.g. increase in TNF $\alpha$ ).

## 256 Discussion

257 For over 30 years, IVIg has been used in several neurological disorders as an efficient  
258 immunomodulator and anti-inflammatory, reviewed in (10, 48). Yet, the mechanisms of action of  
259 IVIg are poorly understood. In the context of AD, antibodies contained in IVIg could exert their  
260 activities by: (1) binding to a broad spectrum of aggregating and pathological forms of A $\beta$  and tau;  
261 (2) binding to A $\beta$  contained in the blood and promoting the efflux of A $\beta$  from the brain, i.e. the  
262 ‘peripheral sink’ hypothesis; (3) engaging immune-mediated responses involved in the clearance  
263 of A $\beta$ ; (4) attenuating cell-death pathway and protecting neurons against A $\beta$ ; and (5) acting as  
264 immunomodulators potentially through Fc $\gamma$ RIIB and sialylated Fc.

265 It is possible that the efficacy of previous clinical trials using IVIg, administered  
266 peripherally, in mild to moderate AD was limited due to the poor access of IVIg to the brain (6,  
267 12, 14, 49). These trials primarily relied on the immunomodulatory effects of IVIg in the periphery,  
268 with some central effects achieved at high dosages over several months that are likely to be  
269 transient (6, 12, 14, 49). As demonstrated here, transcranial FUS-BBB permeability increased the  
270 bioavailability of IVIg from the blood to the hippocampus, where it reached therapeutic efficacy  
271 at relatively low dosage given intravenously. For the usage of IVIg in clinical trials, lowering the  
272 effective dose required for efficacy can lessen the burden on the availability of IVIg as a natural

273 resource, as it is reliant on human blood donors, and it is in high demand for treating several  
274 neurological diseases (16, 17).

275 We postulated that IVIg, combined with non-invasive FUS-mediated therapeutic delivery to  
276 the hippocampus (26), could enhance treatment efficacy. Over the last decade, safe acoustic  
277 parameters of FUS-induced BBB permeability have been established in animal models and in  
278 human, as recently reviewed in (26). In animal models, the use of safe parameters was shown to  
279 prevent, or minimize, red blood cell extravasation (26). Blood-borne molecules can briefly enter  
280 the brain and be cleared within hours, *i.e.* albumin (50), to 4 days, *i.e.* IgG and IgM (19).  
281 Inflammation has been reported to occur acutely after FUS in some, but not all conditions (51-55).  
282 At longer-term post-FUS, evidence suggest putative beneficial effects of albumin, IgG and IgM in  
283 reducing AD pathology and establishing and that a pro-regenerative milieu (19-21, 26, 56, 57). To  
284 date, in animal models of AD, the long-term effects of single and repeated FUS treatments—even  
285 without the addition of a therapeutic—have led to the reduction of A $\beta$  and tau pathologies, and to  
286 the promotion of hippocampal neurogenesis, parenchymal nerve growth factor content, TrkA-  
287 related survival signaling pathways, and cognitive functions (20, 21, 32, 34, 58-63). When  
288 acoustic settings are selected to avoid edema and microbleeds, the restoration of the BBB post-  
289 FUS occurs between 6 to 24 hours in animal models, and in patients with AD and amyotrophic  
290 lateral sclerosis (ALS) (19, 23-28, 31). Recent clinical trials have described FUS-induced BBB  
291 permeability as safe, reproducible, and transient in people with AD and ALS (27-29, 64). Here,  
292 we provide further evidence that two FUS treatments by themselves reduce A $\beta$  plaque pathology,  
293 and we discovered that combined with IVIg, FUS can further enhance treatment efficacy in  
294 reducing the pro-inflammatory cytokine TNFa and promoting neurogenesis in the hippocampal  
295 formation of a Tg mouse model of AD.

296 Our bioavailability data demonstrate that one administration of 0.4 g IVIg /kg (12 mg per  
297 Tg mouse, *i.v.*) resulted in 489 ng IVIg/mg of protein in FUS-targeted hippocampi, compared to  
298 undetectable levels in non-FUS-targeted hippocampi, at four hours post-treatment. In these  
299 conditions, FUS allowed on average 0.09% of the dose of IVIg injected *i.v.* to enter the  
300 hippocampus. A study by St-Amour et al. (15) demonstrated that of 1.5 g IVIg/kg (25 mg per  
301 mouse, *i.p.*) in C57Bl/6 mice delivered 12.5 ng IVIg/mg of protein to the hippocampus, the  
302 equivalent of 0.0017% of the injected dose. As such, FUS delivery translates in an approximate  
303 39-fold greater delivery to the hippocampus (489 ng/mg vs 12.5 ng/mg) by using less than half the  
304 dose administered peripherally (*i.p.*) (12 mg vs 25 mg). Furthermore, it remains possible that we  
305 did not capture the maximal levels of IVIg levels reaching FUS-targeted hippocampi post-FUS for  
306 three main reasons. Firstly, the timeline of FUS-induced BBB permeability (23, 25, 65) could have  
307 led to the accumulation of IVIg in the targeted hippocampi at a time-point that we did not captured  
308 between 4h and 24 h. Secondly, the saline perfusion, aimed to remove IVIg still circulating in the  
309 blood and avoid confounding results, may have also cleared some of the IVIg from the  
310 hippocampal tissue. Thirdly, IVIg was delivered at two defined FUS spots to the hippocampus,  
311 hence underestimating the amount of IVI in ng/mg delivered at each FUS spots by measuring IVIg  
312 in total hippocampal tissue. Increasing the number of FUS spots to target the entire hippocampal  
313 formation would be of interest to address this potential limitation in measurement of  
314 bioavailability. The clearance of IVIg from the FUS-targeted hippocampi at 7 days post-treatment  
315 is in-line with the previously established half-life of IVIg in the hippocampus by St-Amour, *et al.*  
316 (15), i.e. 140 hours (5.8 days).

317 Two-photon microscopy analyses demonstrated that, in response to FUS, amyloid-coated  
318 vessels in 6 to 8-month-old Tg mice have reduced permeability and a limited capacity for change  
319 in diameter compared to measurements observed in nTg mice (66). In contrast, the levels of GAD

320 enhancement, visualized by MRI following FUS-induced BBB permeability, are not significantly  
321 different between Tg and nTg mice (21, 31, 34, 67). Congruent with this data, the amount of  
322 therapeutic, *i.e.* IVIg (current study) and D3 (34), found in targeted brain areas post-FUS is similar  
323 between Tg and nTg mice. In patients with AD, FUS-induced BBB modulation is reported to be  
324 safe, and achievable repeatedly with predictable detection of GAD enhancement to visualize the  
325 increase BBB permeability within few minutes and its restoration within 24 h (28, 29).

326 The pharmacokinetics (PK) of IVIg-FUS delivery in the current study has limitations. For  
327 example, each FUS spot has variability in response to BBB permeability in time and space. The  
328 current experimental design did not account for these variables; the resected tissue for  
329 bioavailability analysis was taken at the same time point for all animals and included larger volume  
330 of tissue relative to the two FUS spots targeted for IVIg delivery. These characteristics are bound  
331 to introduce greater variability in IVIg measurements delivered by FUS compared to a traditional  
332 PK evaluation of a compound homogeneously crossing the BBB. The increased IVIg delivery by  
333 FUS and clearance by 7 days supported the notion of testing two weekly IVIg-FUS bilateral  
334 treatments on treatment effects on A $\beta$  plaque pathology and neurogenesis in both hippocampi.

335 With regards to neurogenesis, a previous study reported that 8 months of IVIg administration  
336 at a high dose (1.0 g/kg/week, *i.v.*; cumulative dose of 32 g/kg) increased the number of immature  
337 neurons (DCX+) in the hippocampus of APP/PS1 mice (9). Here, we aimed to improve treatment  
338 efficacy on neurogenesis by delivering IVIg to the hippocampus with FUS, and identify whether  
339 a putative increase in DCX+ cells comes from newly proliferating cells or the enhanced survival  
340 of immature neurons. Considering the data obtained in the bioavailability study, IVIg was  
341 administered at 0.4 g/kg (*i.v.*), weekly, for 2 weeks, with and without FUS-targeting to the  
342 hippocampi. The results clearly show that two IVIg-FUS treatments, each delivering an estimated  
343 489 ng/mg of IVIg to the hippocampus—here representing approximately 0.09% of the injected

344 dose, were sufficient to reach an effective concentration to promote neurogenesis. Indeed, two  
345 treatments of IVIg-FUS, and not IVIg without FUS, increased the proliferation and survival of  
346 newborn cells differentiating into immature neurons. Hippocampal progenitors, contributing to  
347 adult hippocampal neurogenesis, play a critical role in pattern separation, cognitive function and  
348 long-term memory (68-70). Comparing to Puli, *et al.* (9), IVI-FUS treatments reduced the  
349 cumulative effective dose of IVIg from 32 g/kg (1 g/kg/week, *i.v.*) to 0.8 g/kg (0.4 g/kg/week, *i.v.*)  
350 to promote neurogenesis. In Puli, *et al.* (9), the 8-month IVIg treatment increased the number of  
351 DCX+ cells by less the 2-fold compared to saline. Here, two IVIg-FUS treatments quadrupled the  
352 number of BrdU/DCX+ cells in the hippocampus compared to saline. FUS alone had been  
353 previously characterized as increasing adult hippocampal neurogenesis through cell proliferation,  
354 maturation and survival (i.e., augmenting the numbers of BrdU+, DCX+, and BrdU/NeuN+ cells)  
355 (20-22, 71). Here we found that the main effects of IVIg-FUS are in augmenting cell proliferation  
356 (BrdU+), maintaining differentiation and survival of newborn neurons (BrdU/DCX+). The levels  
357 of hippocampal neurogenesis induced by IVIg-FUS were 4-, 3- and 1.5-fold higher than in Tg  
358 mice treated with saline, IVIg alone, and FUS alone, respectively. This is remarkable considering  
359 that exercise, one of the most potent modulators of neurogenesis, does not significantly increase  
360 hippocampal neurogenesis in Tg mice running between 3 and 4 months of age (39), which would  
361 represent a similar timeline to the current study. Furthermore, running typically results in maximal  
362 increases in hippocampal neurogenesis by 2- to 3-fold (72), *i.e.* considerably below the 4-fold  
363 increase observed here. In light of recent clinical trials using FUS to modulate the BBB in patients  
364 with AD (28, 29), elucidating the effects of FUS, alone and combined with therapeutics, in the  
365 hippocampus is critical. Adult neurogenesis declines rapidly with age and AD (73-75), and we  
366 here provide novel evidence on the capacity of IVIg to potentiate hippocampal neurogenesis in  
367 combination with FUS.

368 The beneficial effects of IVIg-FUS treatments on neurogenesis could not be explain solely  
369 by the reduction of A $\beta$  levels in Tg mice, as they were also observed in nTg animals where A $\beta$   
370 pathology is inexistent. Therefore, the promotion of neurogenesis by IVIg-FUS does not require  
371 A $\beta$ -related mechanisms. IVIg has been previously reported to increase synaptic function without  
372 reducing A $\beta$  pathology in Tg2576 mice, providing another example of the effects of IVIg on  
373 neuronal plasticity independently of A $\beta$  reduction (76). Taken together, our data suggest that the  
374 beneficial effects of IVIg-FUS on neurogenesis, and IVIg on A $\beta$  plaque pathology—found to be  
375 equally efficient with or without FUS—could be mediated by distinct modulation of central  
376 (hippocampus) and peripheral (blood) inflammation, respectively. Previous work has shown that  
377 repeated IVIg administration does not increase anti-human IgG response in mice (7). Instead, IVIg  
378 alters the inflammatory environment (10). Therefore, the changes of peripheral (serum) CCTFs  
379 seen in our work is attributed to immunomodulation effect of IVIg, which can contribute to  
380 reducing A $\beta$  plaque pathology as observed in IVIg treatments alone. Conversely, neurogenesis is  
381 most likely to be modulated directly in the hippocampus, where IVIg and FUS combined alter the  
382 microenvironment. Notably, we found that IVIg-FUS treatments decreased the pro-inflammatory  
383 TNFa, known to inhibit adult neurogenesis (46). TNFa can also influence A $\beta$  pathologies and  
384 cognitive deficits in murine models of AD (77, 78).

385 Our data reveal that IVIg-FUS decreased TNFa and increased CCL5 in the hippocampus of  
386 Tg mice compared to IVIg treatment alone. In addition, IVIg-FUS therapy increased serum TNFa,  
387 CCL4 and CCL5, and decreased serum CCL7 in Tg animals. It is clear that factor responsible for  
388 increases in CCL4, IL2 and GM-CSF in the serum is IVIg and not FUS. CCL4, CCL5 and CCL7  
389 are chemokines that regulate monocyte and T-cell entry into the brain and, along with TNFa, can  
390 be modulated by IVIg (79-82). Furthermore, CCL5, which is increased both in the serum and the  
391 hippocampus, has been associated with cognitive benefits of exercise and is lowered in the serum

392 of AD patients (83-85). Therefore, IVIg-FUS may modulate the chemotactic signaling and  
393 transmigration of monocytes and T-cells by reversing the lowered levels of serum CCL5 in Tg  
394 animals.

395 IVIg-FUS also decreased hippocampal TNF $\alpha$  and increased serum TNF $\alpha$  in Tg animals. Our  
396 data indicate that combined IVIg-FUS treatments modify the equilibrium of TNF $\alpha$  centrally and  
397 peripherally. The mechanisms leading to reduced TNF $\alpha$  in the hippocampus and increased TNF $\alpha$   
398 in the serum remain to be identified, including potential exchanges of TNF $\alpha$  through the BBB  
399 (86). Elevated serum levels of TNF $\alpha$  (>100 pg/ml) have been shown to induce pro-inflammatory  
400 signaling in the blood and brain (87). IVIg-FUS increased TNF $\alpha$  levels in the serum to 50 pg/ml,  
401 which did not globally transform the hippocampal milieu as pro-inflammatory. Other studies have  
402 shown that elevated hippocampal TNF $\alpha$  promotes A $\beta$  production (88-90), and reduces  
403 neurogenesis (91). IVIg injected into the brain of APP/PS1 mice reduced the relative gene  
404 expression of TNF $\alpha$  (92). Here, IVIg-FUS treatments decreased hippocampal A $\beta$  plaque load,  
405 similarly to IVIg treatments alone. In contrast, delivering IVIg to the hippocampus non-invasively  
406 with FUS led to additional beneficial effects known to influence cognitive outcomes, e.g.  
407 decreasing TNF $\alpha$  and promoting neurogenesis. For examples, IVIg-FUS could counteract the  
408 deleterious impact of TNF $\alpha$  on neuronal excitability underlying cognitive functions in Tg mice  
409 (93, 94). Augmenting the dose of IVIg to the brain with FUS, could improve novel object  
410 recognition memory and reduce anxiety-like behavior, as seen in 3xTg-AD mice following chronic  
411 IVIg delivery at a high dose of 1.5 g/kg (9-27 *i.p.* injections) (7). And finally, it has been  
412 demonstrated that inducing a  $\geq 2$ -fold increase in proliferation/survival of hippocampal progenitor  
413 cells in Tg mice can be accompanied by enhanced cognitive function (39). Therefore, our data  
414 strongly suggest that by increasing the bioavailability of IVIg to the hippocampus with FUS,

415 leading to a reduction of TNF $\alpha$  and increase in neurogenesis by 3-fold, IVIg-FUS has the potential  
416 to improve cognitive function and memory.

417 In summary, we found that at a low dose, IVIg administered *i.v.* did not cross the BBB in  
418 significant amounts; and while two IVIg treatments *i.v.* reduced A $\beta$  pathology, they did not  
419 increase hippocampal neurogenesis nor reduced TNF $\alpha$ . In contrast, IVIg *i.v.* combined with FUS-  
420 targeted BBB permeability delivered significant amounts of IVIg to the hippocampus, decreased  
421 TNF $\alpha$  and promoted neurogenesis; while also harnessing the effects of IVIg alone (*i.v.*), reducing  
422 A $\beta$  plaque pathology, and modulating serum CCTFs. Given the potential of FUS to reversibly  
423 modulate the BBB in patients with AD (28, 29), our results suggest a novel approach for the use  
424 of IVIg in AD and other neurological diseases, where the BBB poses a limitation for effective  
425 therapeutic delivery and efficacy.

## 426 **Materials & Methods**

427 All data discussed is included in the manuscript and its supporting information, and it was  
428 generated as per methodology described here.

## 429 **Animals**

430 The TgCRND8 (Tg) mouse model of amyloidosis overexpresses the human amyloid  
431 precursor protein (APP) 695 containing the KM670/671NL and V717F mutations under control of  
432 the hamster prion promoter. By 90 days of age, amyloid plaque deposits in the forebrain are evident  
433 (36, 95). A total of 107 Tg and 116 nTg animals, sex-balanced and age matched, were used for the  
434 bioavailability and repeated efficacy studies. 48 Tg and non-transgenic (nTg) were used for the  
435 bioavailability study, starting at the age of 97-128 days and sacrificed at four different time points  
436 assessed in both genotypes (4 hours, 24 hours, 7 days, 14 days; n=6 per group) for IVIg  
437 quantification. 59 Tg and 68 nTg were used in the efficacy study at the age of  $104 \pm 2$  days for  
438 treatments and sacrificed at 21 days post treatment for both immunohistochemistry and

439 biochemical tissue processing. All animals were bred and housed at Sunnybrook Research  
440 Institute. All experiments were carried out in accordance to the guidelines provided by the Animal  
441 Care Committee at Sunnybrook Research Institute and the Canadian Council on Animal Care and  
442 Animals for Research Act of Ontario.

### 443 **MRI-guided FUS for targeted BBB permeability**

444 On the day of the experiment, animals underwent anesthesia with isoflurane, followed by  
445 depilation of the head, and tail vein catheterization for drug delivery. While under anesthesia,  
446 animals were placed in dorsal recumbancy on a positioning sled, which was placed inside the 7T  
447 MRI (BioSpin 7030; Bruker, Billerica, Massachusetts) for T2 and T1 weighted image acquisition  
448 (20, 21, 96, 97). The sled was fitted on the FUS system with the animal's head resting in a degassed  
449 water bath and positioned above a spherical FUS transducer (1.68 MHz, 75 mm diameter and 60  
450 mm radius of curvature). The transducer was built-in with a small custom PVDF hydrophone in  
451 the center of the transmit transducer (97, 98). The acquired T2 weighted image was registered with  
452 the FUS transducer for bilateral hippocampal targeting in the x, y and z plane. Once the brain  
453 regions to target were identified, Definity microbubbles (0.02 ml/kg; Lantheus Medical Imaging,  
454 North Billerica, Massachusetts) were injected intravenously at the onset of sonication for BBB  
455 permeabilization (1 Hz burst repetition frequency, 10 msec bursts, 120 seconds in total). With the  
456 use of a feedback controller, the sonications were controlled and allowed for consistent BBB  
457 permeabilization irrespective of skull thickness and vasculature variability between subjects (97,  
458 98). Following ultrasound sonication, gadolinium-based MRI contrast agent, Gadodiamide  
459 (Omniscan 0.5 mM/ml, GE Healthcare, Mississauga, ON, Canada) and IVIg where applicable  
460 (Gammagard Liquid 10%, Baxter, Deerfield, Illinois, USA) were injected at the dose of 0.2 ml/kg  
461 and 0.4 g/kg respectively. Post-sonication, animals were returned to the MRI for T1-weighted

462 image acquisition to confirm the BBB permeabilization through Gadodiamide entry into the brain  
463 parenchyma, as visualized as signal hyper-intensity or enhancement.

464 *Bioavailability study:* Using the FUS parameters listed above, nTg and Tg animals were  
465 administered 0.4 g/kg IVIg intravenously and the left side of the brain was targeted by FUS, under  
466 MRI guidance. Specifically, two FUS spots were used per brain region, namely the left  
467 hippocampus and cortex, while the right side of the brain was used as the internal control.

468 *Treatment efficacy study:* Tg and nTg animals were divided into one of four treatment groups,  
469 namely saline, IVIg, FUS or IVIg-FUS. IVIg-FUS animals were treated as outlined above. Four  
470 hippocampal targets were used, two in each dorsal hippocampus. Animals treated with only IVIg  
471 or saline were anesthetized, depilated and injected with the respective treatment through a tail vein  
472 catheter, without undergoing MRI or FUS sonication. Post-treatment, all animals were injected  
473 with 5-bromo-2-deoxyuridine (BrdU, 50 mg/kg) for four consecutive days followed by a second  
474 treatment on day 8. Matlab software (Mathworks, Natick, Massachusetts, USA) was used to  
475 quantify enhancement via measuring pixel intensity of a 2x2 mm area within the region of interest  
476 (four FUS focal spots). This was done using gadolinium-enhanced T1 weighted MRI images  
477 acquired after FUS treatment. The intensity was averaged over the four spots per animal and  
478 compared between Tg and nTg to ensure consistency in BBB permeabilization between genotypes.

#### 479 **Biochemical analyses**

480 The animals were anesthetized using an intraperitoneal injection of ketamine (200 mg/kg)  
481 and xylazine (25 mg/kg), blood was collected from the right ventricle for serum collection followed  
482 by intracardial perfusion (left ventricle) with 0.9% saline. The brain tissue was rapidly dissected,  
483 and flash frozen in liquid nitrogen. The serum samples and dissected brain tissue was stored at -  
484 80°C until further use.

485 *Human IgG ELISA*: For bioavailability study, the snap frozen hippocampus and cortex tissue was  
486 homogenized in lysis buffer and lysates were analyzed using species-specific enzyme-linked  
487 immunosorbent assay (ELISA) using IgG Fc-specific antibodies for capture and the corresponding  
488 HRP-conjugated antibodies for detection (Jackson ImmunoResearch Laboratories Inc.).

489 *Chemokines and trophic factors (CCTFs)*: Half of the homogenized hippocampal and cortical  
490 tissue was sent for analysis to Eve Technologies for a multiplexing laser bead assay (Mouse  
491 Cytokine/Chemokine Array 31-Plex and TGF-beta 3-plex) for an exploratory study design. The  
492 following 36 analytes were targeted: CCL11 (Eotaxin), G-CSF, GM-CSF, M-CSF, IFN $\gamma$ , IL1 $\alpha$ ,  
493 IL1 $\beta$ , IL2, IL3, IL4, IL5, IL6, IL7, IL9, IL10, IL12 (p40), IL12 (p70), IL13, IL15, IL17A, CXCL10  
494 (IP10), CXCL1 (KC), LIF, LIX, MCP1 (CCL2), CXCL9 (MIG), CCL3 (MIP1a), CCL4 (MIP1b),  
495 CXCL2 (MIP2), CCL5 (RANTES), TNF $\alpha$ , VEGF, LIX, TGF $\beta$ 1, TGF $\beta$ 2 and TGF $\beta$ 3. The  
496 experimental conditions and the technology itself minimize potential non-specific binding and  
497 detection, including from endogenous biotin. Specifically, the target analyte is detected by a  
498 capture antibody attached to a fluorescent bead and a detection antibody attached to the  
499 streptavidin-phycoerythrin reporter. Furthermore, several analytes were undetectable (i.e. G-CSF,  
500 M-CSF, IFN $\gamma$ , IL-3, IL-5, IL-6, IL12 (p40), LIX, LIF, and MIP-1b), confirming the lack of  
501 significant non-specific detection. Results are reported in pg/ml for analytes that were above  
502 baseline.

503 Serum levels of 20 CCTF factors were evaluated by using a multiple analyte detection system  
504 (FlowCytomix; eBioscience Inc.) as per kit instructions. The factors measured were: IL-1 $\alpha$ , IL-2,  
505 IL-4, IL-5, IL-6, IL-10, IL-13, IL-17 A/F, IL-18, IL-23, CXCL-1 (KC), GM-CSF, MCP-1 (CCL-  
506 2), MCP-3 (CCL-7), CCL-4 (MIP-1b), CCL-3 (MIP-1a), CCL-5 (RANTES), CXCL-10 (IP-10),

507 IFN $\gamma$ , and TNF $\alpha$  Flow cytometric analysis was performed using FACS Calibur (BD Biosciences)  
508 and detected results were reported in pg/ml.

### 509 **Immunohistochemistry**

510 All animals were sacrificed for tissue collection 21 days after the treatment paradigm began.  
511 Animals were deeply anesthetized using an intraperitoneal injection of ketamine (200 mg/kg) and  
512 xylazine (25 mg/kg), followed by intracardial perfusion with 0.9% saline and 4%  
513 paraformaldehyde (PFA). Whole brains were collected and post-fixed in 4% PFA overnight before  
514 transfer to 30% sucrose at 4°C and kept until the brains sank to the bottom. Brains were cut into  
515 serial 40  $\mu$ m-thick coronal sections using a sliding microtome (Leica). A systematic sampling  
516 method was used to select sections at an interval of 12 throughout the hippocampus (from 0.94  
517 mm to 2.92 mm posterior of Bregma) for immunohistochemistry.

518 *Immunohistochemistry protocol:* Sections used for A $\beta$  plaques were first incubated in a blocking  
519 solution (1% bovine serum, 2% donkey serum and 0.35% Triton-X100 in PBS) for 1 hour.  
520 Following blocking, sections were incubated in mouse 6F3D antibody targeting human A $\beta$  (1:200;  
521 Dako North American Inc.) overnight at 4°C. Subsequently, sections were washed in PBS and  
522 incubated in donkey anti-mouse-Cy3 and donkey anti-goat-Cy5 (1:200; Jackson ImmunoResearch  
523 Laboratories Inc) for 1 hour, washed in PBS and mounted on slides.

524 For IVIg staining, sections were incubated in 3% hydrogen peroxide for 10 minutes, rinsed,  
525 and incubated overnight in biotinylated primary antibody against human IgG (1:100; Santa Cruz,  
526 Product SC2775, Lot G0212). Following PBS rinse, sections were incubated in streptavidin-  
527 conjugated horseradish peroxidase (HRP) (1:1000; Jackson ImmunoResearch Laboratories Inc.,  
528 Product 016030084, Lot 82330) and 3,3-diaminobenzidine (DAB kit; Sigma). Sections were

529 mounted on slides, dehydrated by serial treatment in ethanol and propanol solutions, and  
530 coverslipped.

531 For BrdU and doublecortin (DCX) and staining, sections were incubated in blocking serum  
532 (10% donkey serum and 0.25% Triton-X100 in PBS) for 1 hour. After blocking, sections were  
533 incubated with a goat anti-mouse DCX antibody (1:200; Santa Cruz) for 48 hours. This was  
534 followed by washes in PBS and incubation in donkey anti-goat Alexa 488 (1:200; Jackson  
535 ImmunoResearch Laboratories Inc.) for 2 hours. Sections were subsequently rinsed and treated  
536 with 2N HCl (37°C, 35 minutes) for antigen retrieval, followed by neutralization through  
537 treatment with 0.1M borate buffer (pH 8.5). Post neutralization, sections were rinsed with PBS  
538 and incubated overnight in rat anti-mouse BrdU antibody (1:400; AbD Serotec). Next day, sections  
539 were rinsed and incubated in donkey anti-rat Cy3 (1:200) for 1 hour. This was followed by PBS  
540 rinses and sections were mounted on slides.

541 Confocal imaging and analysis: For IVIg immunoreactivity in the bilateral hippocampus,  
542 brightfield virtual montages were acquired using a 20x objective (0.8 NA) on a Zeiss Axioplan 2  
543 microscope and the 2D Virtual Slice module of Stereo Investigator 10 (MBF BioScience,  
544 Williston, Vermont, USA). For rest of the immunofluorescence imaging, a spinning disk confocal  
545 microscope (CSU-W1; Yokogawa Electric, Zeiss Axio Observer.Z1 - Carl Zeiss) was used to  
546 acquire Z-stack images of the entire hippocampus. Using the tiling feature of the Zen 2012 software  
547 version 1.1.2 (Carl Zeiss), a composite image of the hippocampus was created in three dimensions.  
548 For A $\beta$  plaques immunoreactivity quantification, images were acquired using a 20x objective (0.8  
549 NA) in the Cy3 channels and a maximum intensity projection image was generated for analysis in  
550 the ImageJ software. Using the particle analysis feature of ImageJ, the number and area of plaques  
551 in the entire hippocampus was calculated.

552 For BrdU and DCX cell quantification, images were acquired at 63x (1.40 NA) in the Cy3  
553 and Cy2 channels respectively. An observer blinded to treatment using the Zen software carried  
554 out the cell counting for BrdU-positive cells and BrdU/DCX-positive cells. The total number of  
555 BrdU-positive and BrdU/DCX-positive was multiplied by the sampling interval value (1 in 12, 3-  
556 4 sections/animal) in order to estimate of the total number of cells in the entire hippocampus per  
557 animal.

### 558 **Statistical Analysis**

559 Statistical analysis was done in GraphPad Prism 5 and 8 . In bar graphs, data are represented  
560 as mean + standard deviation (SD). GAD enhancements between Tg and nTg were compared with  
561 unpaired t-tests, and no statistical significance was noted. For bioavailability studies, Wilcoxon  
562 matched-pairs signed rank one-tail tests were performed, under the assumption that greater levels  
563 of IVIg will be found in FUS-treated regions. Significant differences were noted at  $p < 0.05$ . For the  
564 efficacy of two treatments (Saline, IVIg, FUS, IVIg-FUS), one-way analysis of variance (ANOVA)  
565 was used to compare all treatment groups to each other for IVIg immunoreactivity,  $A\beta$  total plaque  
566 number, mean size and surface area, BrdU-positive and BrdU/DCX-positive cells. Newman-Keuls  
567 method was applied as post-hoc analysis and differences were significant at  $p < 0.05$ . For analysis  
568 of CCTFs in the brain and serum, we asked the question of how IVIg-FUS treatment compared to  
569 IVIg alone and FUS treatment compared with saline alone. Therefore, unpaired t-tests were carried  
570 out for each comparison and significant differences reported at  $p < 0.05$ . For the serum analysis of  
571 TNF $\alpha$ , CCL4, IL-2, and GM-CSF, differences between treatment groups were analyzed using non-  
572 parametric Mann-Whitney test (due to a high proportion of zero values) and significance set at  
573  $p < 0.05$ .

574

575 **Acknowledgements**

576 We thank Kristina Mikloska for support with FUS experiments, Shawna Rideout-Gros for  
577 assistance with animal care, and Melissa Theodore for genotyping and animal husbandry. Drs.  
578 Paul Fraser, David Westaway, and Peter St George-Hyslop supplied breeding pairs of TgCRND8  
579 mice. This research was undertaken, in part, thanks to funding from the Canada Research Chairs  
580 program (IA, JM, KH). This work was supported by the Weston Brain Institute and the Canadian  
581 Institutes of Health Research (IA, FRN 137064, 166184). Additional funding was received from  
582 the FDC Foundation, the WB Family Foundation, Gerald and Carla Connor. Salary support was  
583 awarded through a Canadian Blood Services Graduate Fellowship (SD).

584

585 **References**

- 586 1. Alzheimer's Association, Alzheimer's disease facts and figures. *Alzheimer's & Dementia*  
587 **14**, 367-429 (2018).
- 588 2. N. Baazaoui, K. Iqbal, A Novel Therapeutic Approach to Treat Alzheimer's Disease by  
589 Neurotrophic Support During the Period of Synaptic Compensation. *J Alzheimers Dis* **62**,  
590 1211-1218 (2018).
- 591 3. L. Hromadkova, S. V. Ovsepian, Tau-Reactive Endogenous Antibodies: Origin,  
592 Functionality, and Implications for the Pathophysiology of Alzheimer's Disease. *J Immunol*  
593 *Res* **2019**, 7406810 (2019).
- 594 4. A. Manolopoulos *et al.*, Intravenous Immunoglobulin for Patients With Alzheimer's  
595 Disease: A Systematic Review and Meta-Analysis. *Am J Alzheimers Dis Other Demen* **34**,  
596 281-289 (2019).
- 597 5. J. Magga *et al.*, Human intravenous immunoglobulin provides protection against Abeta  
598 toxicity by multiple mechanisms in a mouse model of Alzheimer's disease. *J*  
599 *Neuroinflammation* **7**, 90 (2010).
- 600 6. R. Dodel *et al.*, Intravenous immunoglobulin for treatment of mild-to-moderate  
601 Alzheimer's disease: A phase 2, randomised, double-blind, placebo-controlled, dose-  
602 finding trial. *Lancet Neurol.* **12**, 233-243 (2013).
- 603 7. I. St-Amour *et al.*, IVIg protects the 3xTg-AD mouse model of Alzheimer's disease from  
604 memory deficit and Abeta pathology. *J Neuroinflammation* **11**, 54 (2014).
- 605 8. I. St-Amour, F. Cicchetti, F. Calon, Immunotherapies in Alzheimer's disease: Too much,  
606 too little, too late or off-target? *Acta Neuropathol.* **131**, 481-504 (2016).

- 607 9. L. Puli *et al.*, Effects of human intravenous immunoglobulin on amyloid pathology and  
608 neuroinflammation in a mouse model of Alzheimer's disease. *J Neuroinflammation* **9**, 105  
609 (2012).
- 610 10. J. D. Lunemann, F. Nimmerjahn, M. C. Dalakas, Intravenous immunoglobulin in  
611 neurology--mode of action and clinical efficacy. *Nat Rev Neurol* **11**, 80-89 (2015).
- 612 11. S. E. Counts, S. E. Perez, B. He, E. J. Mufson, Intravenous immunoglobulin reduces tau  
613 pathology and preserves neuroplastic gene expression in the 3xTg mouse model of  
614 Alzheimer's disease. *Curr Alzheimer Res* **11**, 655-663 (2014).
- 615 12. N. R. Relkin *et al.*, A phase 3 trial of IV immunoglobulin for Alzheimer disease. *Neurology*  
616 **88**, 1768-1775 (2017).
- 617 13. N. Relkin, Clinical trials of intravenous immunoglobulin for Alzheimer's disease. *J Clin*  
618 *Immunol* **34 Suppl 1**, S74-79 (2014).
- 619 14. S. Kile *et al.*, IVIG treatment of mild cognitive impairment due to Alzheimer's disease: a  
620 randomised double-blinded exploratory study of the effect on brain atrophy, cognition and  
621 conversion to dementia. *J. Neurol. Neurosurg. Psychiatry* **88**, 106-112 (2017).
- 622 15. I. St-Amour *et al.*, Brain bioavailability of human intravenous immunoglobulin and its  
623 transport through the murine blood-brain barrier. *J. Cereb. Blood Flow Metab.* **33**, 1983-  
624 1992 (2013).
- 625 16. D. A. Loeffler, Should development of Alzheimer's disease-specific intravenous  
626 immunoglobulin be considered? *J Neuroinflammation* **11**, 198 (2014).
- 627 17. E. E. Perez *et al.*, Update on the use of immunoglobulin in human disease: A review of  
628 evidence. *J. Allergy Clin. Immunol.* **139**, S1-S46 (2017).
- 629 18. A. W. Zuercher, R. Spirig, A. Baz Morelli, T. Rowe, F. Käsermann, Next-generation Fc  
630 receptor-targeting biologics for autoimmune diseases. *Autoimmun. Rev.* **18**, 102366 (2019).

- 631 19. J. F. Jordão *et al.*, Amyloid- $\beta$  plaque reduction, endogenous antibody delivery and glial  
632 activation by brain-targeted, transcranial focused ultrasound. *Experimental Neurology* **248**,  
633 16-29 (2013).
- 634 20. T. Scarcelli *et al.*, Stimulation of hippocampal neurogenesis by transcranial focused  
635 ultrasound and microbubbles in adult mice. *Brain Stimul* **7**, 304-307 (2014).
- 636 21. A. Burgess *et al.*, Alzheimer disease in a mouse model: MR imaging-guided focused  
637 ultrasound targeted to the hippocampus opens the blood-brain barrier and improves  
638 pathologic abnormalities and behavior. *Radiology* **273**, 736-745 (2014).
- 639 22. J. Shin *et al.*, Focused ultrasound-induced blood-brain barrier opening improves adult  
640 hippocampal neurogenesis and cognitive function in a cholinergic degeneration dementia  
641 rat model. *Alzheimers Res Ther* **11**, 110 (2019).
- 642 23. K. Hynynen, N. McDannold, N. Vykhodtseva, F. A. Jolesz, Noninvasive MR imaging-  
643 guided focal opening of the blood-brain barrier in rabbits. *Radiology* **220**, 640-646 (2001).
- 644 24. M. A. O'Reilly, O. Hough, K. Hynynen, Blood-Brain Barrier Closure Time After  
645 Controlled Ultrasound-Induced Opening Is Independent of Opening Volume. *J Ultrasound*  
646 *Med* **36**, 475-483 (2017).
- 647 25. N. McDannold, N. Vykhodtseva, K. Hynynen, Blood-brain barrier disruption induced by  
648 focused ultrasound and circulating preformed microbubbles appears to be characterized by  
649 the mechanical index. *Ultrasound Med. Biol.* **34**, 834-840 (2008).
- 650 26. Y. Meng *et al.*, Safety and efficacy of focused ultrasound induced blood-brain barrier  
651 opening, an integrative review of animal and human studies. *J Control Release* **309**, 25-36  
652 (2019).
- 653 27. A. Abrahao *et al.*, First-in-human trial of blood-brain barrier opening in amyotrophic lateral  
654 sclerosis using MR-guided focused ultrasound. *Nat Comm* **10**, 4373 (2019).

- 655 28. N. Lipsman *et al.*, Blood-brain barrier opening in Alzheimer's disease using MR-guided  
656 focused ultrasound. *Nat Commun* **9**, 2336 (2018).
- 657 29. A. R. Rezai *et al.*, Noninvasive hippocampal blood-brain barrier opening in Alzheimer's  
658 disease with focused ultrasound. *Proc Natl Acad Sci U S A* **117**, 9180-9182 (2020).
- 659 30. S. B. Raymond *et al.*, Ultrasound enhanced delivery of molecular imaging and therapeutic  
660 agents in Alzheimer's disease mouse models. *PLoS One* **3**, e2175 (2008).
- 661 31. J. F. Jordao *et al.*, Antibodies targeted to the brain with image-guided focused ultrasound  
662 reduces amyloid-beta plaque load in the TgCRND8 mouse model of Alzheimer's disease.  
663 *PLoS One* **5**, e10549 (2010).
- 664 32. R. M. Nisbet *et al.*, Combined effects of scanning ultrasound and a tau-specific single chain  
665 antibody in a tau transgenic mouse model. *Brain* **140**, 1220-1230 (2017).
- 666 33. T. Alecou, M. Giannakou, C. Damianou, Amyloid  $\beta$  plaque reduction with antibodies  
667 crossing the blood-brain barrier, which was opened in 3 sessions of focused ultrasound in  
668 a rabbit model. *J. Ultrasound Med.* **36**, 2257-2270 (2017).
- 669 34. K. Xhima *et al.*, Focused ultrasound delivery of a selective TrkA agonist rescues  
670 cholinergic function in a mouse model of Alzheimer's disease. *Sci Adv* **6**, eaax6646 (2020).
- 671 35. M. Yu *et al.*, Selective impairment of hippocampus and posterior hub areas in Alzheimer's  
672 disease: An MEG-based multiplex network study. *Brain* **140**, 1466-1485 (2017).
- 673 36. M. A. Chishti *et al.*, Early-onset amyloid deposition and cognitive deficits in transgenic  
674 mice expressing a double mutant form of amyloid precursor protein 695. *J Biol Chem* **276**,  
675 21562-21570 (2001).
- 676 37. S. Dudal *et al.*, Inflammation occurs early during the Abeta deposition process in  
677 TgCRND8 mice. *Neurobiol Aging* **25**, 861-871 (2004).

- 678 38. C. Cavanagh *et al.*,  $\beta$ CTF-correlated burst of hippocampal TNF $\alpha$  occurs at a very early,  
679 pre-plaque stage in the TgCRND8 mouse model of Alzheimer's disease. *J. Alzheimers Dis.*  
680 **36**, 233-238 (2013).
- 681 39. E. Maliszewska-Cyna, K. Xhima, I. Aubert, A comparative study evaluating the impact of  
682 physical exercise on disease progression in a mouse model of Alzheimer's disease. *J*  
683 *Alzheimers Dis* **53**, 243-257 (2016).
- 684 40. B. M. Francis *et al.*, Object recognition memory and BDNF expression are reduced in  
685 young TgCRND8 mice. *Neurobiol Aging* **33**, 555-563 (2012).
- 686 41. A. Bellucci *et al.*, Cholinergic dysfunction, neuronal damage and axonal loss in TgCRND8  
687 mice. *Neurobiol Dis* **23**, 260-272 (2006).
- 688 42. S. Krantic *et al.*, Hippocampal GABAergic neurons are susceptible to amyloid-beta toxicity  
689 in vitro and are decreased in number in the Alzheimer's disease TgCRND8 mouse model.  
690 *J Alzheimers Dis* **29**, 293-308 (2012).
- 691 43. S. Krantic, From current diagnostic tools and therapeutics for Alzheimer's disease towards  
692 earlier diagnostic markers and treatment targets. *Curr Alzh Res* **14**, 2-5 (2017).
- 693 44. C. Joao, V. S. Negi, M. D. Kazatchkine, J. Bayry, S. V. Kaveri, Passive serum therapy to  
694 immunomodulation by IVIg: A fascinating journey of antibodies. *J. Immunol.* **200**, 1957-  
695 1963 (2018).
- 696 45. W. A. Sewell, S. Jolles, Immunomodulatory action of intravenous immunoglobulin.  
697 *Immunology* **107**, 387-393 (2002).
- 698 46. A. Borsini, P. A. Zunszain, S. Thuret, C. M. Pariante, The role of inflammatory cytokines  
699 as key modulators of neurogenesis. *Trends Neurosci.* **38**, 145-157 (2015).

- 700 47. J. Kimmelman, J. S. Mogil, U. Dirnagl, Distinguishing between exploratory and  
701 confirmatory preclinical research will improve translation. *PLoS Biol.* **12**, e1001863  
702 (2014).
- 703 48. A. Manolopoulos *et al.*, Intravenous immunoglobulin for patients with Alzheimer's disease:  
704 A systematic review and meta-analysis. *Am. J. Alzheimer's Dis. Other Dementias* **34**, 281-  
705 289 (2019).
- 706 49. R. Dodel *et al.*, Intravenous immunoglobulins as a treatment for Alzheimer's disease:  
707 rationale and current evidence. *Drugs* **70**, 513-528 (2010).
- 708 50. A. Alonso, E. Reinz, M. Fatar, M. G. Hennerici, S. Meairs, Clearance of albumin following  
709 ultrasound-induced blood-brain barrier opening is mediated by glial but not neuronal cells.  
710 *Brain Res.* **1411**, 9-16 (2011).
- 711 51. Z. I. Kovacs *et al.*, MRI and histological evaluation of pulsed focused ultrasound and  
712 microbubbles treatment effects in the brain. *Theranostics* **8**, 4837-4855 (2018).
- 713 52. Z. I. Kovacs *et al.*, Disrupting the blood-brain barrier by focused ultrasound induces sterile  
714 inflammation. *Proc Natl Acad Sci U S A* **114**, E75-E84 (2017).
- 715 53. D. McMahon, C. Poon, K. Hynynen, Evaluating the safety profile of focused ultrasound  
716 and microbubble-mediated treatments to increase blood-brain barrier permeability. *Expert*  
717 *Opin Drug Deliv* **16**, 129-142 (2019).
- 718 54. D. McMahon, R. Bendayan, K. Hynynen, Acute effects of focused ultrasound-induced  
719 increases in blood-brain barrier permeability on rat microvascular transcriptome. *Sci Rep*  
720 **7**, 45657 (2017).
- 721 55. D. McMahon, K. Hynynen, Acute Inflammatory Response Following Increased Blood-  
722 Brain Barrier Permeability Induced by Focused Ultrasound is Dependent on Microbubble  
723 Dose. *Theranostics* **7**, 3989-4000 (2017).

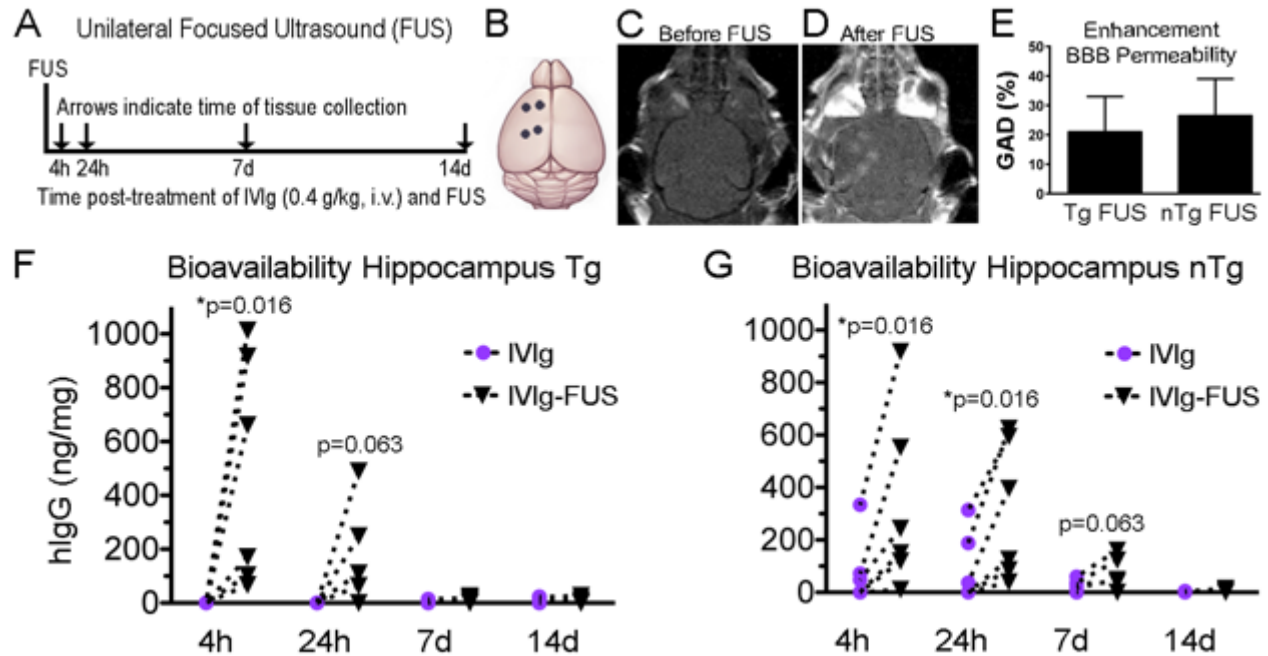
- 724 56. G. Leinenga, J. Gotz, Scanning ultrasound removes amyloid-beta and restores memory in  
725 an Alzheimer's disease mouse model. *Sci Transl Med* **7**, 278ra233 (2015).
- 726 57. J. Silburt, N. Lipsman, I. Aubert, Disrupting the blood-brain barrier with focused  
727 ultrasound: Perspectives on inflammation and regeneration. *Proc Natl Acad Sci U S A* **114**,  
728 E6735-E6736 (2017).
- 729 58. R. Pandit, G. Leinenga, J. Götz, Repeated ultrasound treatment of tau transgenic mice clears  
730 neuronal tau by autophagy and improves behavioral functions. *Theranostics* **9**, 3754-3767  
731 (2019).
- 732 59. P. W. Janowicz, G. Leinenga, J. Götz, R. M. Nisbet, Ultrasound-mediated blood-brain  
733 barrier opening enhances delivery of therapeutically relevant formats of a tau-specific  
734 antibody. *Sci. Rep.* **9**, 9255 (2019).
- 735 60. G. Leinenga, W. K. Koh, J. Götz, Scanning ultrasound in the absence of blood-brain barrier  
736 opening is not sufficient to clear  $\beta$ -amyloid plaques in the APP23 mouse model of  
737 Alzheimer's disease. *Brain Res. Bull.* **153**, 8-14 (2019).
- 738 61. G. Leinenga, J. Gotz, Safety and Efficacy of Scanning Ultrasound Treatment of Aged  
739 APP23 Mice. *Front Neurosci* **12**, 55 (2018).
- 740 62. D. G. Blackmore *et al.*, Multimodal analysis of aged wild-type mice exposed to repeated  
741 scanning ultrasound treatments demonstrates long-term safety. *Theranostics* **8**, 6233-6247  
742 (2018).
- 743 63. M. E. Karakatsani *et al.*, Unilateral focused ultrasound-induced blood-brain barrier opening  
744 reduces phosphorylated tau from the rTg4510 mouse model. *Theranostics* **9**, 5396-5411  
745 (2019).
- 746 64. Y. Meng *et al.*, Glymphatics visualization after focused ultrasound-induced blood-brain  
747 barrier opening in humans. *Ann. Neurol.* **86**, 975-980 (2019).

- 748 65. M. A. O'Reilly *et al.*, Investigation of the Safety of Focused Ultrasound-Induced Blood-  
749 Brain Barrier Opening in a Natural Canine Model of Aging. *Theranostics* **7**, 3573-3584  
750 (2017).
- 751 66. A. Burgess, T. Nhan, C. Moffatt, A. L. Klibanov, K. Hynynen, Analysis of focused  
752 ultrasound-induced blood-brain barrier permeability in a mouse model of Alzheimer's  
753 disease using two-photon microscopy. *J Control Release* **192**, 243-248 (2014).
- 754 67. J. F. Jordão *et al.*, Amyloid-beta plaque reduction, endogenous antibody delivery and glial  
755 activation by brain-targeted, transcranial focused ultrasound. *Exp Neurol* **248**, 16-29  
756 (2013).
- 757 68. C. D. Clelland *et al.*, A functional role for adult hippocampal neurogenesis in spatial pattern  
758 separation. *Science* **325**, 210-213 (2009).
- 759 69. O. Lazarov, M. P. Mattson, D. A. Peterson, S. W. Pimplikar, H. van Praag, When  
760 neurogenesis encounters aging and disease. *Trends Neurosci* **33**, 569-579 (2010).
- 761 70. T. Toda, F. H. Gage, Review: adult neurogenesis contributes to hippocampal plasticity. *Cell*  
762 *Tissue Res.* **373**, 693-709 (2018).
- 763 71. S. J. Mooney *et al.*, Focused Ultrasound-Induced Neurogenesis Requires an Increase in  
764 Blood-Brain Barrier Permeability. *PLoS One* **11**, e0159892 (2016).
- 765 72. C. i. Cooper, H. Y. Moon, H. v. Praag, On the run for hippocampal plasticity. *Csh Perspect*  
766 *Med* **8**, a029736 (2018).
- 767 73. M. K. Tobin *et al.*, Human Hippocampal Neurogenesis Persists in Aged Adults and  
768 Alzheimer's Disease Patients. *Cell Stem Cell* **24**, 974-982 e973 (2019).
- 769 74. E. P. Moreno-Jiménez *et al.*, Adult hippocampal neurogenesis is abundant in neurologically  
770 healthy subjects and drops sharply in patients with Alzheimer's disease. *Nat. Med.* **25**, 554-  
771 560 (2019).

- 772 75. Kirsty L. Spalding *et al.*, Dynamics of hippocampal neurogenesis in adult humans. *Cell*  
773 **153**, 1219-1227 (2013).
- 774 76. B. Gong *et al.*, IVIG immunotherapy protects against synaptic dysfunction in Alzheimer's  
775 disease through complement anaphylatoxin C5a-mediated AMPA-CREB-C/EBP signaling  
776 pathway. *Mol Immunol* **56**, 619-629 (2013).
- 777 77. P. He *et al.*, Deletion of tumor necrosis factor death receptor inhibits amyloid beta  
778 generation and prevents learning and memory deficits in Alzheimer's mice. *J. Cell Biol.*  
779 **178**, 829-841 (2007).
- 780 78. P. Chakrabarty, A. Herring, C. Ceballos-Diaz, P. Das, T. E. Golde, Hippocampal expression  
781 of murine TNFalpha results in attenuation of amyloid deposition in vivo. *Mol.*  
782 *Neurodegener.* **6**, 16 (2011).
- 783 79. D. E. Spaner *et al.*, Association of blood IgG with tumor necrosis factor-alpha and clinical  
784 course of chronic lymphocytic leukemia. *EBioMedicine* **35**, 222-232 (2018).
- 785 80. T. Berger *et al.*, Predicting therapeutic efficacy of intravenous immunoglobulin (IVIG) in  
786 individual patients with relapsing remitting multiple sclerosis (RRMS) by functional  
787 genomics. *J Neuroimmunol* **277**, 145-152 (2014).
- 788 81. S. Rivest, Review A deficiency in CCR 2 + monocytes : the hidden side of Alzheimer ' s  
789 disease. *Journal of Molecular Cell Biology* **5**, 284-293 (2013).
- 790 82. J. Quandt, K. Dorovini-Zis, The beta chemokines CCL4 and CCL5 enhance adhesion of  
791 specific CD4+ T cell subsets to human brain endothelial cells. *J Neuropathol Exp Neurol*  
792 **63**, 350-362 (2004).
- 793 83. M. Haskins, T. E. Jones, Q. Lu, S. K. Bareiss, Early alterations in blood and brain RANTES  
794 and MCP-1 expression and the effect of exercise frequency in the 3xTg-AD mouse model  
795 of Alzheimer's disease. *Neurosci Lett* **610**, 165-170 (2016).

- 796 84. M. I. Kester *et al.*, Decreased mRNA expression of CCL5 [RANTES] in Alzheimer's  
797 disease blood samples. *Clin. Chem. Lab. Med.* **50**, 61-65 (2012).
- 798 85. J. Quandt, K. Dorovini-Zis, The beta chemokines CCL4 and CCL5 enhance adhesion of  
799 specific CD4+ T cell subsets to human brain endothelial cells. *J. Neuropathol. Exp. Neurol.*  
800 **63**, 350-362 (2004).
- 801 86. W. A. Banks, From blood-brain barrier to blood-brain interface: new opportunities for CNS  
802 drug delivery. *Nat. Rev. Drug Discov.* **15**, 275-292 (2016).
- 803 87. S. Biesmans *et al.*, Peripheral administration of tumor necrosis factor-alpha induces  
804 neuroinflammation and sickness but not depressive-like behavior in mice. *Biomed Res Int*  
805 **2015**, 716920 (2015).
- 806 88. D. K. Lahiri *et al.*, Role of cytokines in the gene expression of amyloid beta-protein  
807 precursor: identification of a 5'-UTR-binding nuclear factor and its implications in  
808 Alzheimer's disease. *J. Alzheimers Dis.* **5**, 81-90 (2003).
- 809 89. M. Yamamoto *et al.*, Interferon- $\gamma$  and tumor necrosis factor- $\alpha$  regulate amyloid- $\beta$  plaque  
810 deposition and  $\beta$ -secretase expression in Swedish mutant APP transgenic mice. *Am. J.*  
811 *Pathol.* **170**, 680-692 (2007).
- 812 90. G. Liao, M. Zhang, E. W. Harhaj, S. C. Sun, Regulation of the NF- $\kappa$ B-inducing kinase by  
813 tumor necrosis factor receptor-associated factor 3-induced degradation. *J. Biol. Chem.* **279**,  
814 26243-26250 (2004).
- 815 91. R. E. Iosif *et al.*, Tumor necrosis factor receptor 1 is a negative regulator of progenitor  
816 proliferation in adult hippocampal neurogenesis. *J Neurosci* **26**, 9703-9712 (2006).
- 817 92. T. L. Sudduth, A. Greenstein, D. M. Wilcock, Intracranial injection of Gammagard, a  
818 human IVIg, modulates the inflammatory response of the brain and lowers A $\beta$  in

- 819 APP/PS1 mice along a different time course than anti-Abeta antibodies. *J. Neurosci.* **33**,  
820 9684-9692 (2013).
- 821 93. C. Cavanagh *et al.*, Inhibiting tumor necrosis factor-alpha before amyloidosis prevents  
822 synaptic deficits in an Alzheimer's disease model. *Neurobiol Aging* **47**, 41-49 (2016).
- 823 94. I. Mahar *et al.*, Phenotypic Alterations in Hippocampal NPY- and PV-Expressing  
824 Interneurons in a Presymptomatic Transgenic Mouse Model of Alzheimer's Disease. *Front*  
825 *Aging Neurosci* **8**, 327 (2016).
- 826 95. A. Hanna *et al.*, Age-related increase in amyloid plaque burden is associated with  
827 impairment in conditioned fear memory in CRND8 mouse model of amyloidosis.  
828 *Alzheimers Res Ther* **4**, 21 (2012).
- 829 96. N. P. Ellens *et al.*, The targeting accuracy of a preclinical MRI-guided focused ultrasound  
830 system. *Med. Phys.* **42**, 430-439 (2015).
- 831 97. M. A. O'Reilly, K. Hynynen, Ultrasound and Microbubble-Mediated Blood-Brain Barrier  
832 Disruption for Targeted Delivery of Therapeutics to the Brain. *Methods Mol Biol* **1831**,  
833 111-119 (2018).
- 834 98. M. A. O'Reilly, K. Hynynen, Blood-brain barrier: real-time feedback-controlled focused  
835 ultrasound disruption by using an acoustic emissions-based controller. *Radiology* **263**, 96-  
836 106 (2012).
- 837

838 **Figures**839 **Figure 1**840 **Figure 1 | Focused ultrasound increases the bioavailability of IVIg to the hippocampus.** (A)

841 IVIg (0.4 g/kg) was injected intravenously in transgenic (Tg) and nTg animals. (A, B) A unilateral

842 focused ultrasound (FUS) treatment FUS was done on the left side of the brain. (B) The blood-

843 brain barrier (BBB) was modulated with two FUS spots (black dots) per regions, namely the cortex

844 and hippocampus. The contralateral regions on the right side of the brain served as controls

845 exposed to circulating IVIg without FUS permeabilization. (A) Animals were sacrificed at 4 hours,

846 24 hours, 7 days and 14 days and brain homogenates were analyzed using human IgG (hIgG)

847 ELISA. (C, D) MRI visualization of the brain (C) before and (D) after FUS-BBB opening, which

848 results in noticeable gadolinium (GAD) entry as two lighter spots over the cortex, and two over

849 the hippocampus. (E) No significant difference in GAD enhancement post-FUS, indicative of BBB

850 permeability, was observed between Tg and nTg animals (n=16, p=0.21). hIgG content was found

851 to be higher in FUS-treated hippocampi (left) compared to the untreated hippocampi (right) in Tg

852 mice at 4 hours post-IVIg-FUS delivery (G, \* $p=0.016$ ,  $n=6$ ); and in nTg mice at 4 and 24 hours  
853 treatment (F, \* $p=0.016$ ,  $n=6$  per time-point). T-test was used to compare GAD enhancement.  
854 Bioavailability of IVIg at each independent time-point was analyzed with a Wilcoxon matched-  
855 pairs signed rank one-tail test, under the assumption that greater levels of IVIg will be found in  
856 FUS-treated hippocampi. Significant differences were noted at  $p<0.05$ .  
857

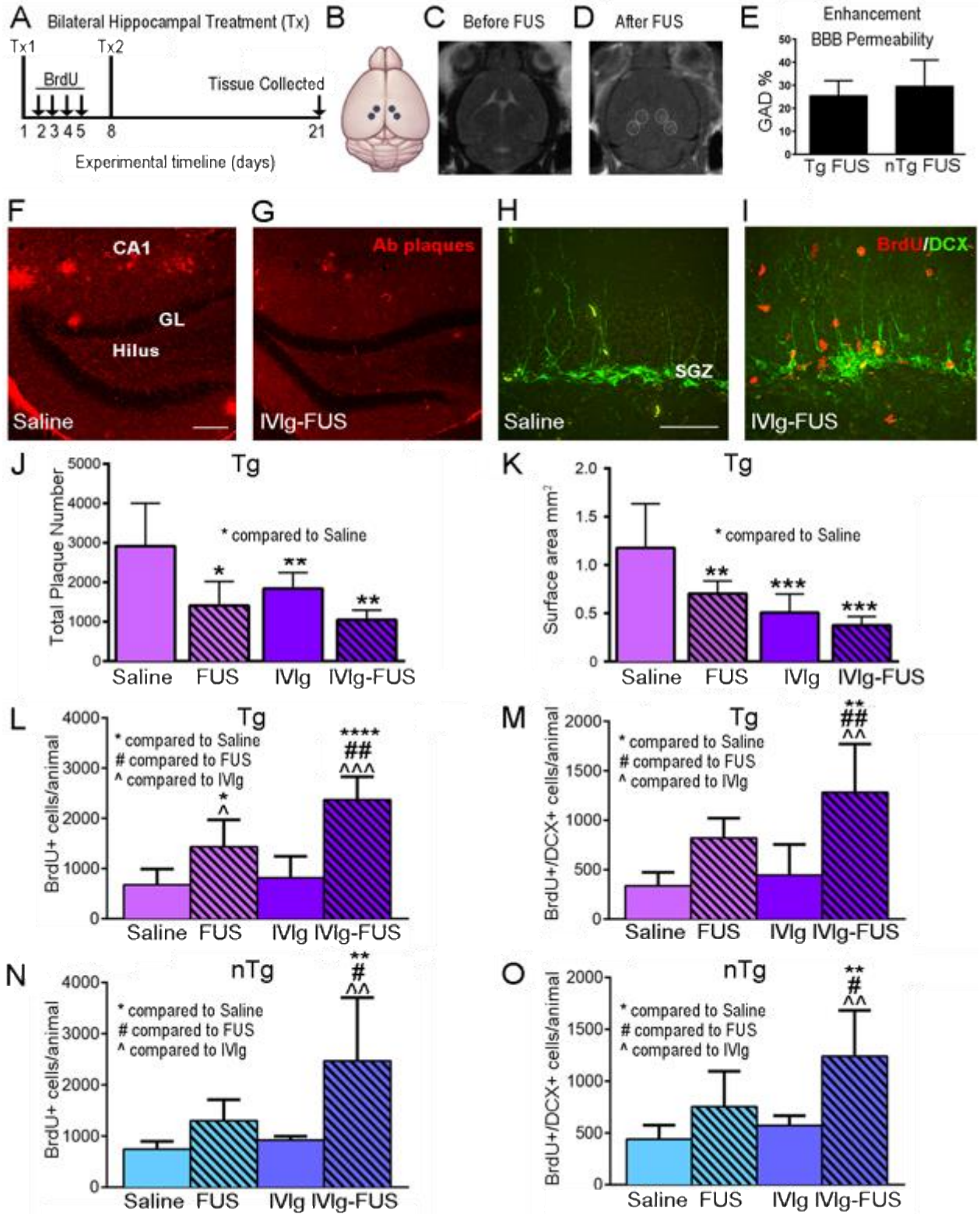


Figure 2

858

859 **Figure 2 | Intravenous IVIg reduces A $\beta$  plaque pathology and promotes neurogenesis only**  
860 **when combined with focused ultrasound.** (A) Experimental timeline of weekly bilateral  
861 treatments (Tx1, Tx2): saline; IVIg alone (0.4 g/kg *i.v.*), focused ultrasound (FUS), IVIg-FUS at  
862 day 1 and 8, with tissue collection at day 21 in Tg and nTg animals. One day after the first treatment  
863 (Tx1), animals were injected intraperitoneally with 5-bromo-2-deoxyuridine (BrdU, 50 mg/kg) for  
864 four consecutive days (arrows) followed by a second treatment (Tx2) on day 8 and tissue collection  
865 on day 21. (B) The hippocampus was targeted bilaterally with four FUS spots. (C, D) MRI  
866 visualization of the brain (C) before and (D) after FUS-BBB opening, which results in noticeable  
867 gadolinium (GAD) entry as four lighter spots over the bilateral hippocampi. (E) No significant  
868 difference in GAD enhancement post-FUS, indicative of BBB permeability, was observed  
869 between Tg and nTg animals ( $p=0.33$ ). (F, G) Representative images of plaques (red) in Tg mice  
870 treated with (F) saline and (G) IVIg-FUS. (H, I) Representative images of BrdU+ cells (red) and  
871 DCX+ cells (green) are shown here in nTg mice treated with (H) saline and (I) IVIg-FUS. (J, K)  
872 A $\beta$  plaque number and surface area were significantly decreased by all treatments (FUS, IVI, and  
873 IVIg-FUS) compared to saline ( $n=5-6$  per group). No statistical difference was found in efficacy  
874 at reducing A $\beta$  plaque pathology between treatments. (L-O) In Tg and nTg animals, IVIg-FUS the  
875 most effective treatment at increasing (L, M) the total number of BrdU+ cells, and (N, O) the only  
876 treatment to significantly increase the number of immature neurons (BrdU+/DCX+) ( $n=5$ ). Data  
877 are shown as mean+SD with one-way ANOVA and Newman-Keuls post-hoc tests. \* $p<0.05$ ,  
878 \*\* $p<0.01$ , \*\*\* $p<0.001$ ; \*compared to saline, # compared to FUS, ^ compared to IVIg. Scale bar:  
879 (F-G) 20  $\mu\text{m}$ ; (H-I) 100  $\mu\text{m}$ .

880

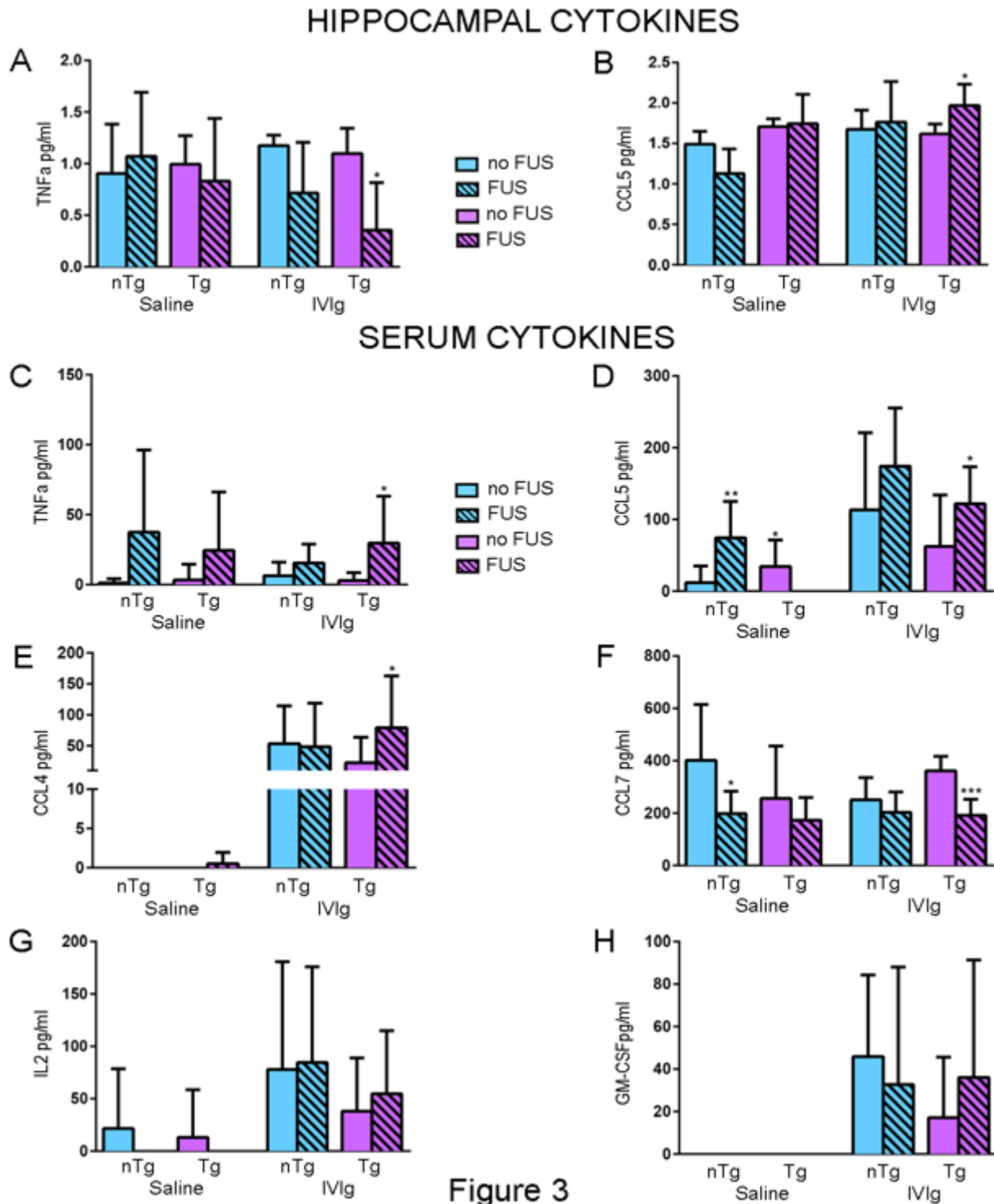
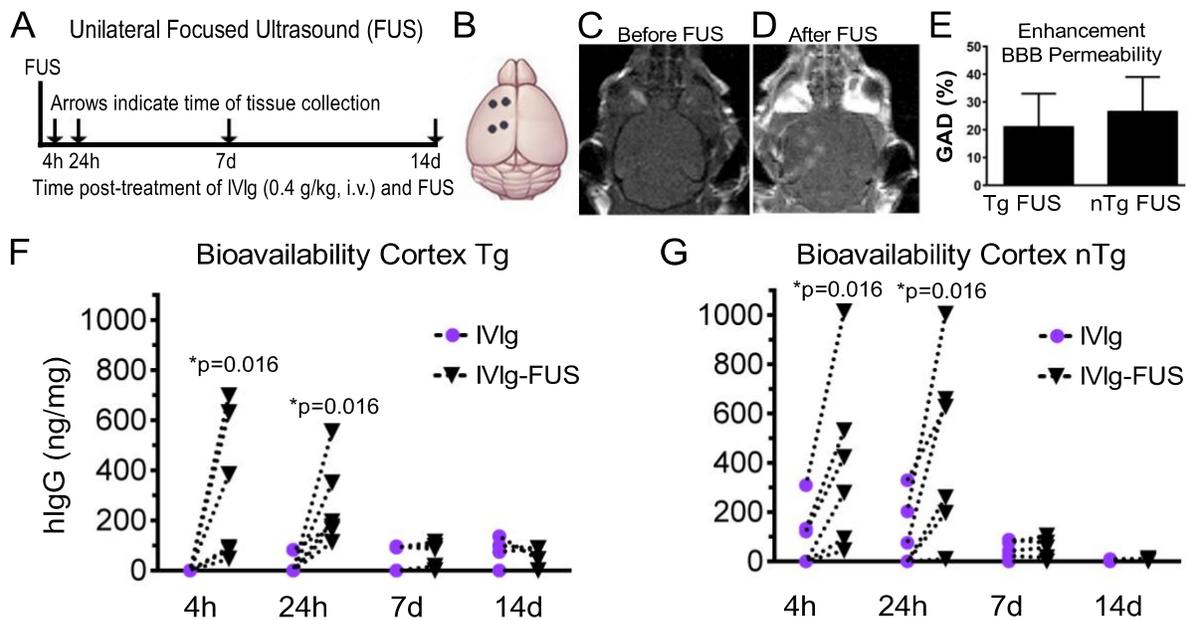


Figure 3

881  
 882 **Figure 3 | IVIg-FUS treatments mediates changes in CCTF levels in the hippocampus and**  
 883 **serum.** (A, B) In Tg mice, IVIg-FUS treatments decreased TNFα and increased CCL5 levels and  
 884 in the hippocampus compared to IVIg treatment alone. (C-E) In the serum, Tg animals treated with

885 IVIg-FUS show increased TNF $\alpha$ , CCL5 and CCL4 compared to IVIg alone. CCL5 levels are also  
 886 increased in FUS treated nTg animals (compared to saline) and saline treated Tg animals  
 887 (compared to FUS). (F) Serum CCL7 is decreased with treatments of IVIg-FUS compared to IVIg  
 888 in Tg animals, and treatments of FUS treatment compared to saline in nTg animals. (G-H) The  
 889 detection of IL2 and GM-CSF was facilitated by IVIg and IVIg-FUS treatments in Tg and nTg  
 890 animals. Brains (n=3-4) and serum (n=9-15) were analyzed using laser bead based multiplex assay  
 891 for CCTF protein quantification. Data are shown as mean+SD with unpaired t-test or Mann  
 892 Whitney U-test, depending on distribution. \*p<0.05, \*\*p<0.01, \*\*\*p<0.001.

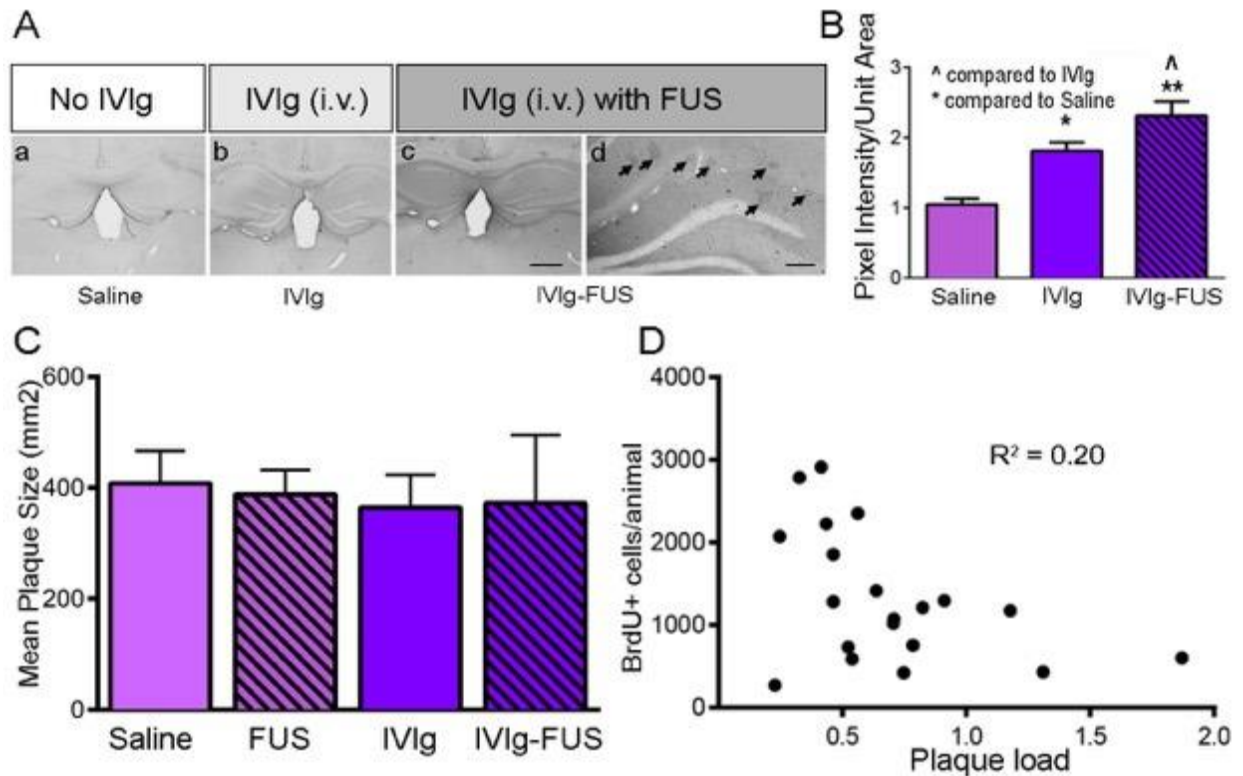
### 893 Supplementary Figures



894

895 **S1 | Focused ultrasound increases the bioavailability of IVIg to the cortex.** (A) IVIg (0.4 g/kg)  
 896 was injected intravenously in transgenic (Tg) and nTg animals. (A, B) A unilateral focused  
 897 ultrasound (FUS) treatment FUS was done on the left side of the brain. (B) The blood-brain barrier  
 898 (BBB) was modulated with two FUS spots (black dots) per regions, namely the cortex and  
 899 hippocampus. The contralateral regions on the right side of the brain served as controls exposed  
 900 to circulating IVIg without FUS permeabilization. (A) Animals were sacrificed at 4 hours, 24  
 901 hours, 7 days and 14 days and brain homogenates were analyzed using human IgG (hIgG) ELISA.  
 902 (C, D) MRI visualization of the brain (C) before and (D) after FUS-BBB opening, which results  
 903 in noticeable gadolinium (GAD) entry as two lighter spots over the cortex, and two over the  
 904 hippocampus. (E) No significant difference in GAD enhancement post-FUS, indicative of BBB

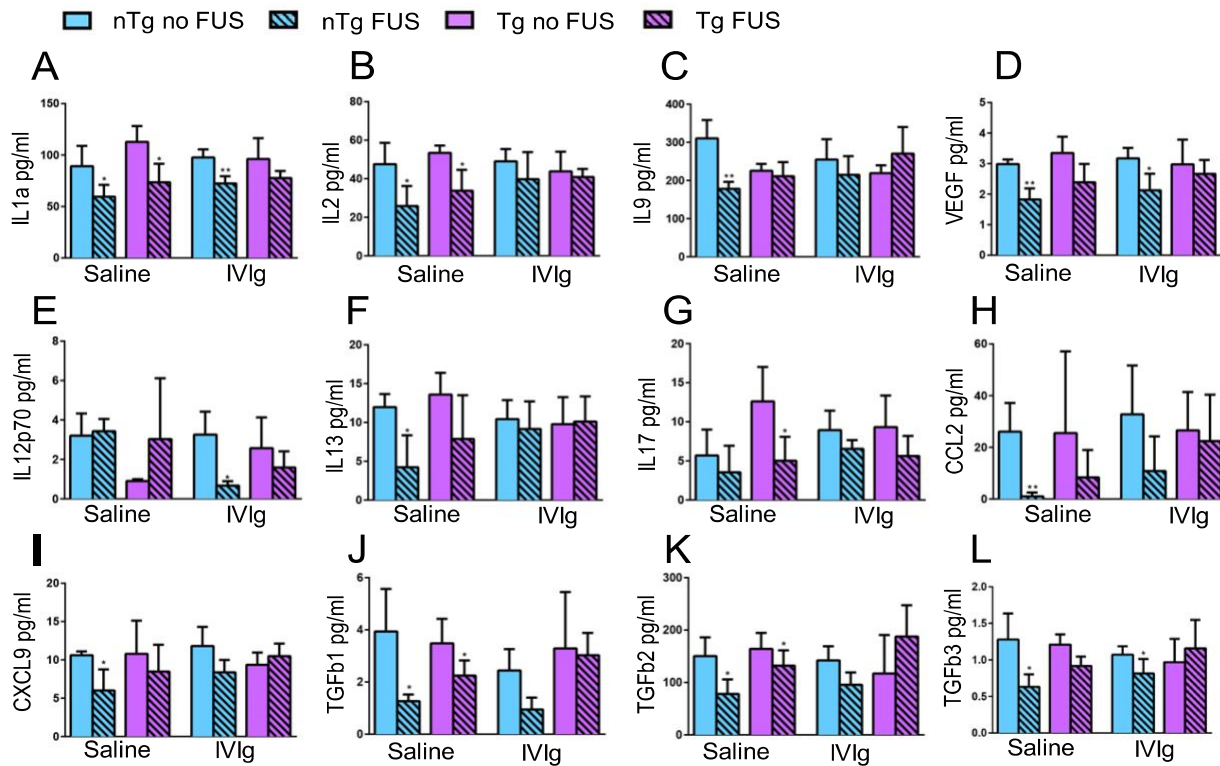
905 permeability, was observed between Tg and nTg animals ( $n=16$ ,  $p=0.21$ ). hIgG content was found  
 906 to be higher in FUS-treated cortex (left) compared to the untreated cortex (right) in Tg mice post-  
 907 IVIg-FUS delivery at 4 hours (G,  $*p=0.016$ ,  $n=6$ , average 323 ng/mg) and 24 hours (G,  $*p=0.016$ ,  
 908  $n=6$ , average 259 ng/mg); and in nTg mice at 4 hours (F,  $*p=0.016$ ,  $n=6$ , average 323 ng/mg) and  
 909 24 hours (F,  $*p=0.016$ ,  $n=6$  per time-point). T-test was used to compare GAD enhancement.  
 910 Bioavailability of IVIg at each independent time-point was analyzed with a Wilcoxon matched-  
 911 pairs signed rank one-tail test, under the assumption that greater levels of IVIg will be found in  
 912 FUS-treated hippocampi. Significant differences were noted at  $p<0.05$ .



913  
 914 **S2 | IVIg biodistribution, plaque size and lack of correlation between A $\beta$  plaque pathology**  
 915 **and proliferating hippocampal cells.** (A) Representative images of animals injected  
 916 intravenously (i.v.) with (a) saline, No IVIg; (b) IVIg; and (c, d) IVIg combined with focused  
 917 ultrasound (IVIg-FUS) bilaterally to the hippocampus. IVIg entering the brain binds to A $\beta$  plaques,  
 918 here visible by immunohistochemistry (d, arrows). (B) At 21 days post-treatments, the levels of  
 919 human IgG immunoreactivity in bilateral hippocampi were higher in IVIg-FUS compared to IVIg  
 920 alone and saline alone. IVg alone also had higher levels of immunoreactivity of human IgG  
 921 compared to saline alone ( $n=3$  per group). (C) No difference in mean plaque size in the  
 922 hippocampus of Tg animals treated with FUS, IVIg and IVIg-FUS was found ( $n=5-6$  per group).  
 923 (D) There was no significant correlation between plaque load, *i.e.* surface area of A $\beta$  plaques, and  
 924 cell proliferation (BrdU+) in the hippocampus ( $R^2=0.20$ ). Data are shown as mean+SD with one-  
 925 way ANOVA analysis with Newman-Keuls post-hoc tests  $^{\wedge}p<0.05$ ,  $^{**}p<0.01$ ; \*compared to  
 926 saline,  $^{\wedge}$ compared to IVIg. (A) Scale bars (a-c) 50  $\mu$ m, (d) 20  $\mu$ m.

927

### HIPPOCAMPAL CYTOKINES



928

929 **S3 | Alterations in CCTFs occur primarily in hippocampi treated with focused ultrasound.**

930 (A-K) Hippocampal tissue from the treated animals (n=3-4) was analyzed using laser bead based  
 931 multiplex assay for CCTFs protein quantification. The levels of CCTFs for IVIg-FUS treated  
 932 animals were compared to IVIg, and FUS treated animals were compared to saline control. Data  
 933 are shown as mean+SD with unpaired t-test or Mann Whitney U-test, depending on distribution.  
 934 \*p<0.05, \*\*p<0.01, \*\*\*p<0.001.